CHAPTER NINE

9. THE NERRIGUNDAH EXPERIMENTAL CATCHMENT

The objective of setting up an experimental catchment at the property known as "Nerrigundah", was to collect soil moisture and standard meteorological data, for a field application of the soil moisture profile estimation algorithm established in Chapter 6. This data was collected with an emphasis on obtaining near-surface soil moisture measurements for updating of the simplified soil moisture profile model developed in Chapter 7, using the Modified Kalman-filter assimilation scheme proposed in Chapter 8. Moreover, measurements of the soil moisture profile were obtained for evaluation of the soil moisture profile estimation algorithm. This data was used for both one-dimensional (Chapter 10) and three-dimensional (Chapter 11) field applications of the soil moisture profile estimation algorithm.

In an operational setting, only standard meteorological data will be available for forcing of the hydrologic model. Hence, only standard meteorological data were used in evaluation of the actual evapotranspiration and precipitation rates. Moreover, only published elevation and soil data will be available for input to the hydrologic model in an operational system. Although field measured elevation and soil data were used in the spatially distributed field application presented in Chapter 11, published elevation and soil data is provided for comparison with the field measured data, and an analysis of expected errors presented. The CD-ROM accompanying this thesis contains a copy of the data collected in the Nerrigundah catchment.

9.1 FIELD SITE SELECTION

In selecting a catchment for collection of the experimental data required for the field application, a number of items were considered. From a data collection and modelling view point, it was desirable to monitor a complete (sub)catchment of less than 10 ha occupied by pasture in undulating terrain (15%

Figure 9.1: Photograph of Nerrigundah catchment looking from east to west.

maximum slope) with some interesting topographical features, containing relatively rock free soil that was not too hard.

A catchment area greater than 10 ha was felt to be too large for monitoring soil moisture content with an adequate spatial resolution, while the remaining restrictions stemmed from the proposed data collection system. The spatial distribution of near-surface soil moisture content was to be collected using TDR probes fitted to an all terrain vehicle with a **D**ifferential **G**lobal **P**ositioning **S**ystem (DGPS) for locating sample/measurement sites. Thus, terrain slopes greater than 15% were considered too steep for adequate vehicle stability, whilst hard soils and soil containing rocks make insertion of the TDR probes difficult, lifting the vehicle off the ground. Moreover, rock in the soil has been found to interfere with TDR measurements of soil moisture content. In addition, the catchment had to be free from irrigation, artificial drainage, dams, or other unnatural sources of soil moisture content.

The Nerrigundah experimental catchment is located in the Williams River catchment on a property called Nerrigundah, approximately 11 km north-west of Dungog, NSW, Australia. The catchment runs east to west with a relief of 27 m. Hillslopes are typically 11% with a range from 3% to 22%, and the main drainage line has an average slope of 9% with a range from 1% to 17%. The catchment has an elevation of approximately 110 m **A**ustralian **H**eight **D**atum (AHD) and is used for grazing of beef cattle (Figure 9.1).

The catchment is situated on a variant of the Tillegra Erosional Landscape, which is located on the Wooton Beds. The Wooton Beds consist of sandstone, siltstone, claystone, shale, limestone and lavas, dating from the Carboniferous

period (New South Wales Department of Mines, 1966). In this soil landscape, the soil is usually shallow (30 to 90 cm) consisting of well to moderately well drained Bleached Loams, Structured Loams and Lithosols on siltstone parent material, with the occasional moderately deep to deep patch (55 to 290 cm) consisting of well to imperfectly drained Soloths, Solodic soils and yellow Podzolic soils on sandstone (Henderson, 1999).

Nerrigundah has a temperate climate with a mean annual summer dominant rainfall of 1000 mm and a class A pan evaporation of 1600 mm. The maximum mean monthly rainfall occurs in January (147 mm) and the minimum occurs in July (37 mm), while the maximum mean monthly pan evaporation occurs in December (225 mm) and the minimum occurs in June (60 mm). Mean summer maximum and minimum temperatures are 30°C and 16°C respectively and mean winter maximum and minimum temperatures are 15°C and 6°C respectively (Australian Bureau of Meteorology, 1988).

To verify that the Nerrigundah catchment was producing anticipated soil moisture patterns in response to rainfall, a transect across the catchment was monitored from June 17 1996 to September 25 1996. Soil moisture measurements were made every 10 m with the Soil Moisture Equipment Corporation TRASE TDR System using 15 cm connector TDR probes. The standard TRASE calibration was used to determine the volumetric soil moisture content from the measured dielectric constant (Soil Moisture Equipment Corporation, 1989). Soil moisture measurements were made on Julian days 169, 178, 184, 197, 201, 211, 234 and 269 (see Table B.1 in Appendix B for a Julian day of year calender). As no rainfall measuring device had been installed in the catchment at this time, rainfall measurements were obtained from two nearby rain stations, located on either side of the Nerrigundah catchment. The results from this monitoring are given in Figure 9.2, whilst the location of these raingauges with respect to the Nerrigundah catchment is given in Figure 9.3 and the location of the transect within the experimental catchment is indicated in Figure 9.4.

Transect monitoring results displayed anticipated soil moisture patterns and response to rainfall. At the start of monitoring (mid winter), the entire transect

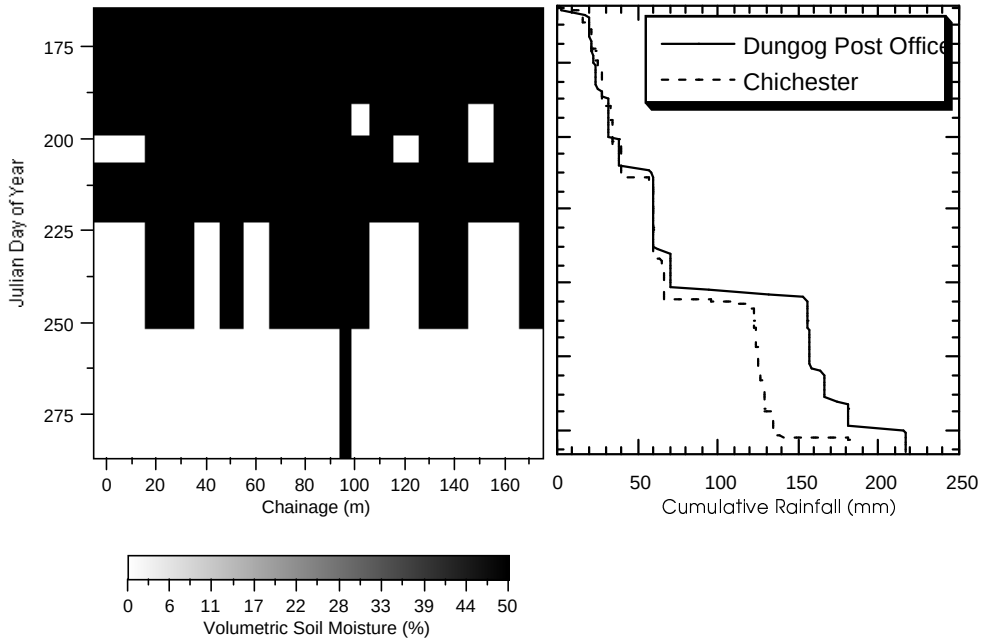

a)

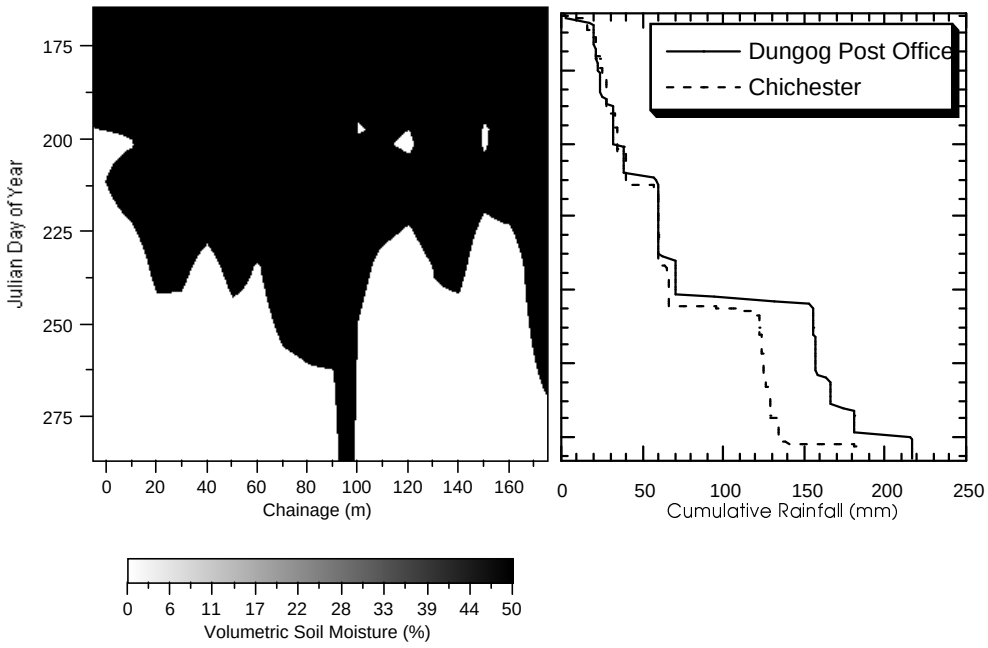

b)

Figure 9.2: Volumetric soil moisture content along the monitoring transect and cumulative rainfall during preliminary monitoring period: a) raw measurement soil moisture content image; b) interpolated soil moisture image content.

was relatively moist. The catchment remained in this state until spring approached, at which time the hillslopes and ridges began drying out, with the gully (chainage 95 m) remaining consistently wetter. Figure 9.2 also displays the wetting up of the transect in response to the rainfall on Julian day 209. Unfortunately, Figure 9.2 does not show the catchment wetting up in response to the 60 to 90 mm of rainfall around Julian day 242. This wetting up is not seen

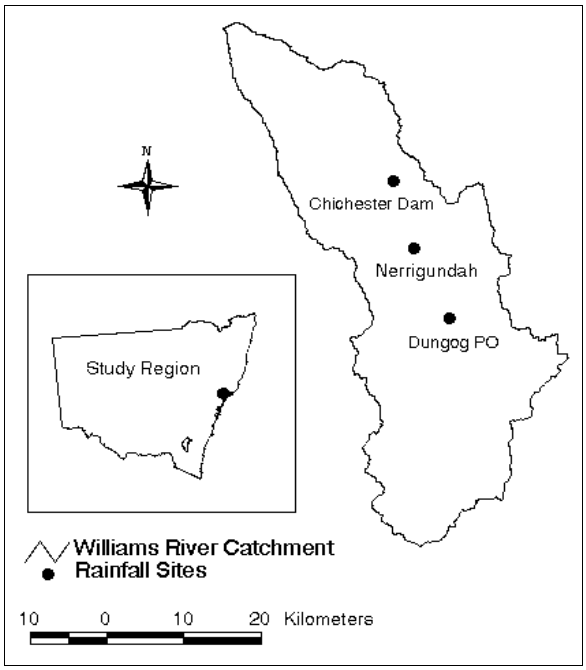

Figure 9.3: Location of Bureau of Meteorology raingauges with respect to the Nerrigundah experimental catchment.

because the measurements on Julian day 234 were before the rainfall event, and the following measurements on Julian day 269 were 27 days after the rainfall event. However, Figure 9.2 does indicate a lull in the rate of catchment drying, which could have resulted from the re-wetting of the catchment.

9.2 DIGITAL ELEVATION MODEL

An accurate **D**igital **E**levation **M**odel (DEM) of the Nerrigundah catchment was generated from a Total Station field survey, with horizontal coordinates on the **A**ustralian **M**ap **G**rid (AMG) and elevations on AHD (Andre Kable and Mark Scanlan, Personal Communication).

Approximately 4600 elevation data points were observed with an average spacing of 7.5 m. In addition to the elevation data for the experimental catchment and its surrounds, the survey located fences, buildings, dams, trees/shrubs, monitoring equipment and soil sample locations (Figure 9.4).

Elevation data was also available from a published DEM obtained from the Land Information Centre, Bathurst, NSW, Australia (Figure 9.5). These published DEMs are produced by digitising the contours on existing 1:25 000 topographical maps and fitting a bi-cubic spline through the data points.

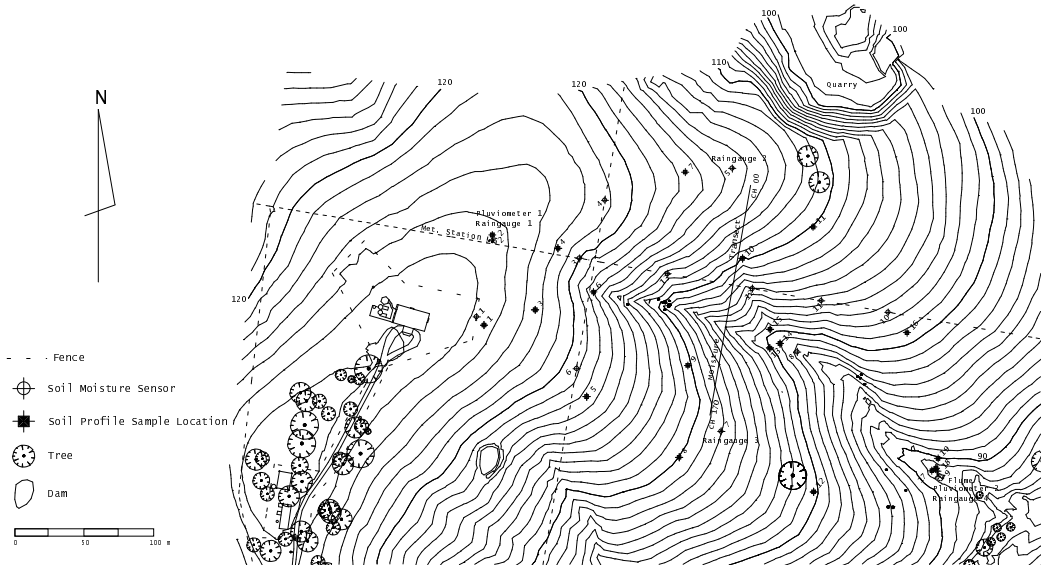

Figure 9.4: Accurate DEM for the Nerrigundah catchment.

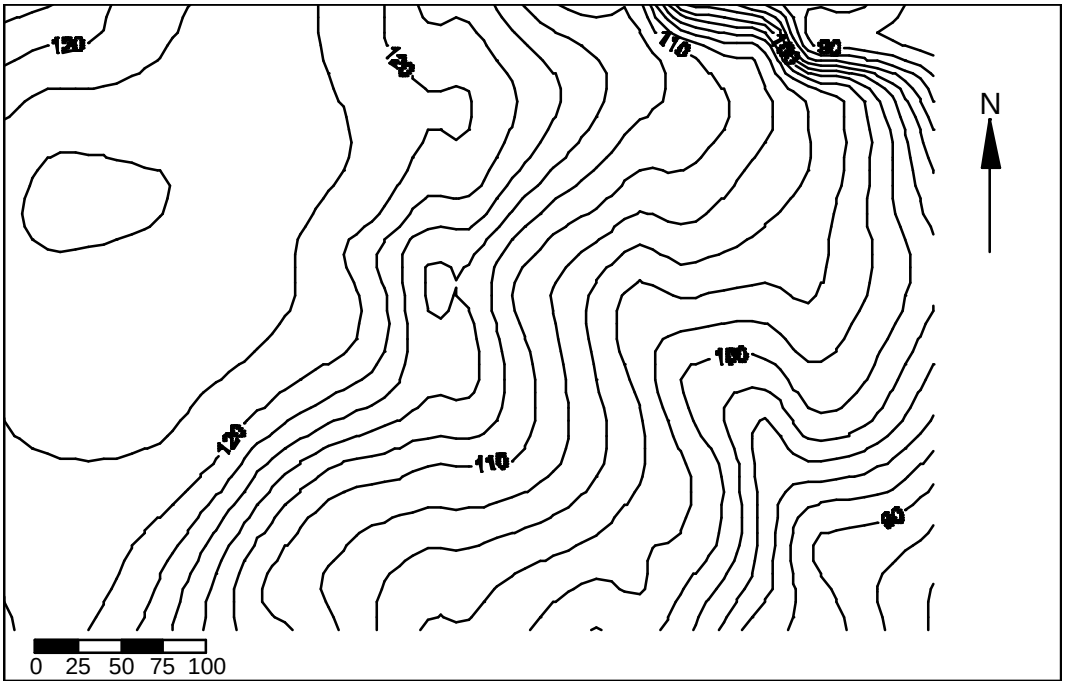

Figure 9.5: Published DEM for the Nerrigundah catchment.

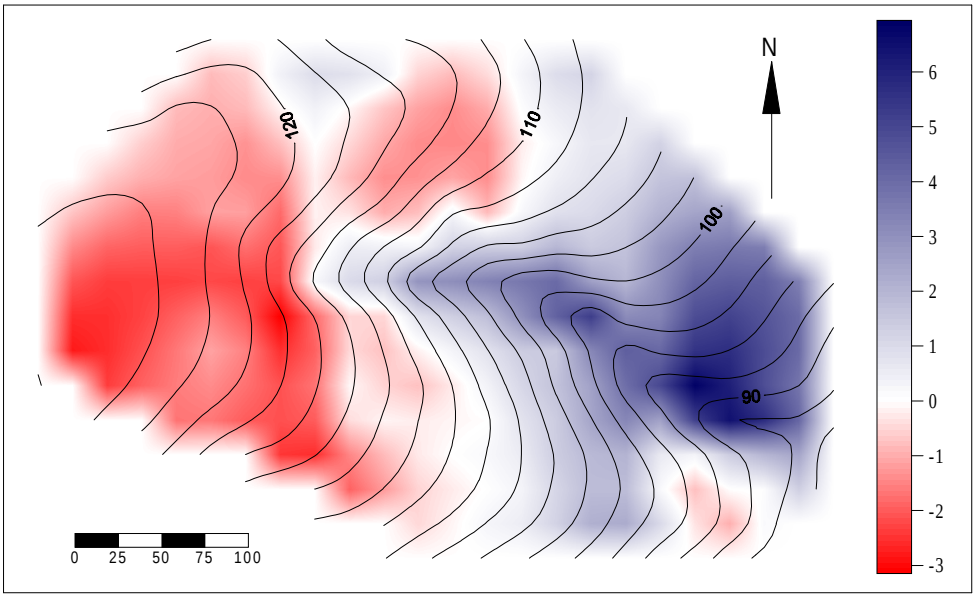

a)

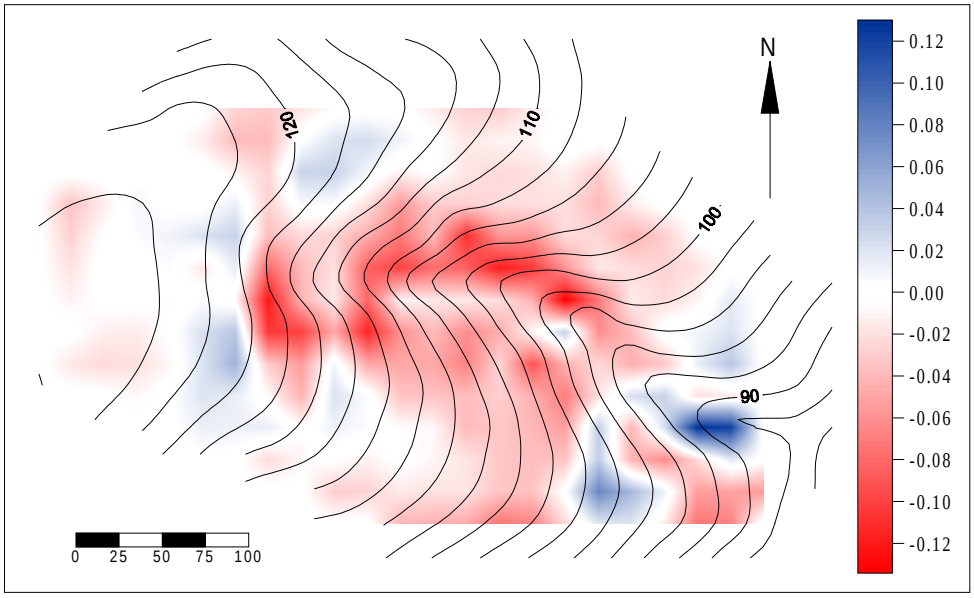

b)

Figure 9.6: Errors in the published DEM: a) elevations (m); b) slopes (m/m).

A statistical analysis of the published DEM accuracy was performed by comparing the elevations of common grid points with the more accurate DEM from ground survey. This comparison was made for elevations interpolated onto a 20 m × 20 m grid, the same grid used for the collection of near-surface soil moisture data, and modelling of catchment soil moisture profiles in Chapter 11.

The spatial distribution of these errors in elevation and DEM derived slope are given in Figure 9.6. For elevation, negative errors are aggregated in the upper

Table 9.1: Statistical results from comparison of the published DEM with the more accurate DEM from the ground survey.

Statistical Parameter	***Elevations (m)***	***Slopes (m/m)***
Mean Difference	0.059	–0.019
Absolute Mean Difference	1.735	0.030
RMS Error	2.177	0.040
Standard Deviation	2.179	0.035
Correlation Length	193.7±5.9	25.7±1.4
Maximum Difference	6.939	0.130
Minimum Difference	–4.487	–0.130

reaches of the catchment while positive errors are aggregated in the major drainage path and lower reaches of the catchment (Figure 9.6a). The net effect of this is a reduction in the range of elevation from the top to the bottom of the catchment, and hence a reduction in slope. Moreover, negative errors in elevation are approximately half as large as the positive errors in elevation. The errors in slope (Figure 9.6b) show that the range of both positive and negative errors are approximately equal and that the largest errors are located along the intersections of adjacent areas of large positive and large negative errors in elevation, as would be expected. Whilst errors in elevation are concentrated in two main areas, the errors in slope are not.

The statistical parameters that have been evaluated in this analysis of the published DEM are: (i) the mean difference between the elevations and slopes; (ii) the absolute mean difference in elevation and slope; (iii) the root mean square error in elevation and slope; (iv) the standard deviation of errors in elevation and slope; and (v) the correlation length of errors in elevation and slope.

The results from this statistical analysis (Table 9.1) show that whilst on average there is only a small difference in elevation between the two surfaces, the error is up to 7 m at some grid points. The statistical results also show that on average there is an error of approximately 2 m in absolute elevation at any grid point within the catchment for the published elevation data, with a correlation length of approximately 190 m. This correlation length of errors in elevation is

likely to be representative of the spacing of data points from which the contours on the topographic map were derived.

The long correlation length of elevation errors relative to the grid point spacing would suggest that whilst there are significant errors in absolute elevation, the errors in relative elevation between surrounding grid points, and hence derived slopes, should be much reduced. This is confirmed by Table 9.1, with slope errors of approximately 3% at any grid point, and a correlation length of approximately 25 m. However, maximum errors in terrain slope are as large as ±13%. The short correlation length of slope errors is characteristic of the spacing from which both estimates of slope were derived. The characteristics of the DEM errors are similar to those found by Walker and Willgoose (1999).

Apart from slopes, the other factor that influences modelling of the catchment from the published DEM is the drainage directions and hence drainage network. Figure 9.7 shows a comparison of the drainage network from both the ground truth DEM and the published DEM. This comparison shows that the published DEM correctly identifies most of the main drainage line, with a close match between the drainage networks on the northern half of the catchment. However, this match is not so good for the southern half of the catchment.

When comparing the DEM derived drainage network with the contours, both drainage networks appear equally acceptable. The areas of the catchment in which the drainage network from the published DEM does not compare well with the contours is at the catchment divide and near the catchment outlet. At the catchment divide, the drainage network for the published DEM extends slightly over the crest, while at the outlet, the drainage network has incorrectly identified the main drainage line.

9.3 CATCHMENT MONITORING AND INSTRUMENTATION

The Nerrigundah experimental catchment was permanently instrumented from October 12 1996 through to October 20 1998, for soil moisture content and soil temperature, and surface soil moisture and heat fluxes. The permanent instrumentation was located such that lateral redistribution of soil moisture would

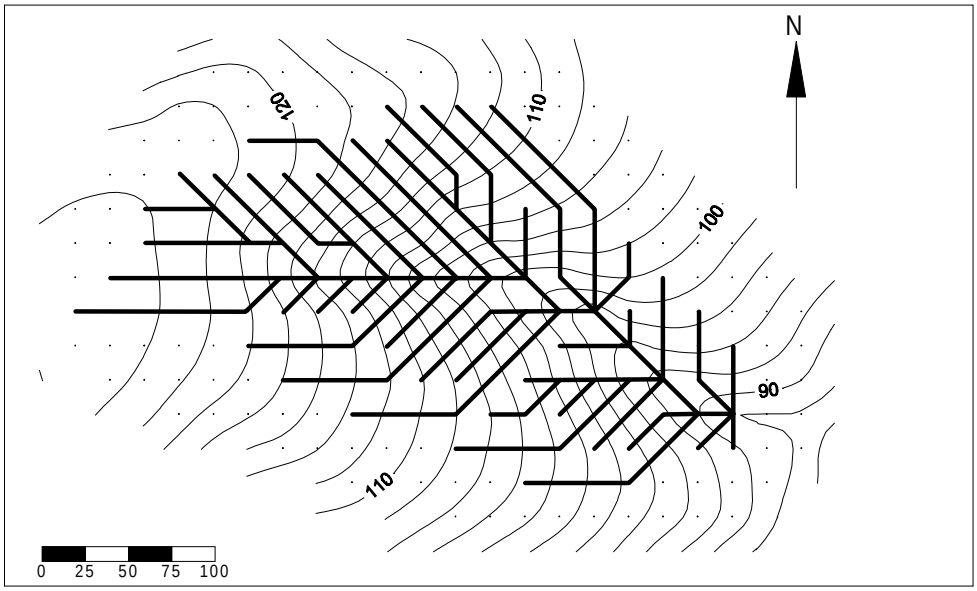

a)

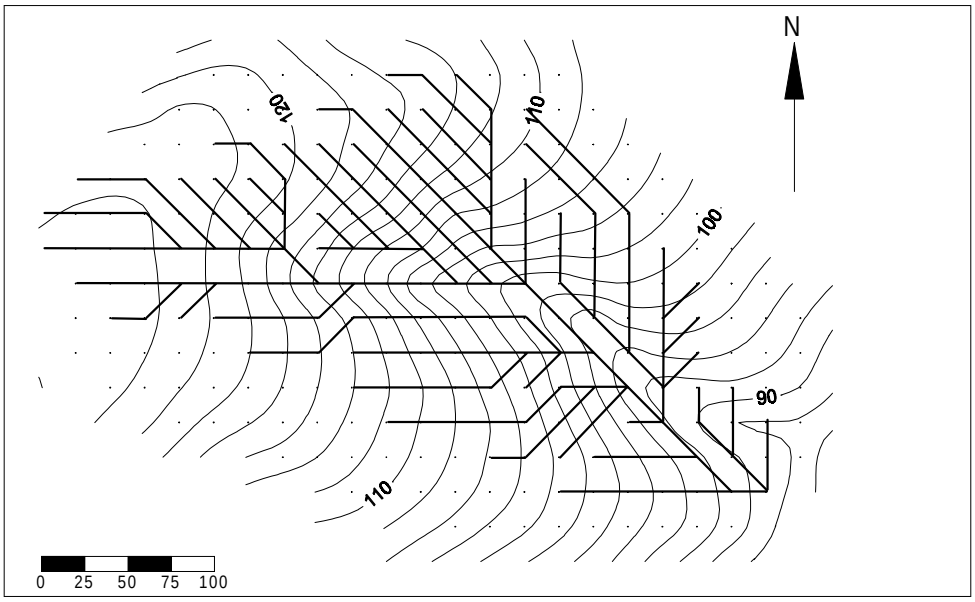

b)

Figure 9.7: Comparison of contours and drainage paths from: a) ground truth DEM; and b) published DEM.

be negligible, and measurements for estimating the surface fluxes (precipitation/evapotranspiration) representative of the entire catchment. The requirement of no lateral redistribution was for the one-dimensional field application of the soil moisture profile estimation algorithm (Chapter 10). Therefore, the permanent instrumentation was located in a level location in the upper reaches of the catchment (Figure 9.4).

Evaluation of the soil moisture profile estimation algorithm at the catchment scale (Chapter 11) required knowledge of the spatial variation of soil moisture profiles, while updating of the hydrologic model required observations of the spatial distribution in near-surface soil moisture content. Monitoring of this spatial data could not be performed economically using permanent instrumentation. Hence, the spatial and temporal variation of both near-surface soil moisture content and soil moisture over the soil profile was extensively monitored during an intensive field campaign from August 27 1997 to September 22 1997. Monitoring of soil moisture profiles was continued from September 22 1997 to October 20 1998, for calibration of the catchment scale soil moisture profile model, developed in Chapter 7. Soil moisture profiles were measured on August 22 1997 to provide background soil moisture values for the intensive field campaign.

9.3.1 PERMANENT INSTRUMENTATION

Permanent instrumentation in the Nerrigundah catchment consisted of a Campbell Scientific automatic weather station which monitored: relative humidity and air temperature; soil temperature at 0.5, 1, 2, 4, 6, 8, 12, 16, 24, 32 and 40 cm depths using thermocouples; soil heat flux at 2 and 12 cm depths using soil heat flux plates; atmospheric pressure; precipitation; net radiation; wind speed; and soil moisture content at a depth of 5 cm using a Campbell Scientific CS615 probe inserted horizontally, providing a soil moisture measurement over a layer thickness of approximately 4 cm (Campbell Scientific Inc., 1995). Apart from rainfall, all measurements were made at 1 minute intervals, and the average was logged every ten minutes. Rainfall was recorded for each tip of the 0.2 mm tipping bucket. The total soil profile depth of this location was approximately 46 cm. Soil temperature data were used for determining the soil heat flux at the soil surface, which was used to evaluate the Penman-Monteith potential evapotranspiration (section 9.4.1.2).

The soil moisture profile was continuously monitored using five Virrib soil moisture sensors installed horizontally at depths of 10, 15, 20, 30 and 40 cm, providing soil moisture measurements over a layer thickness of 12 cm (Komin, Technical Data). These measurements were logged every 15 minutes. In addition,

soil moisture measurements were made in this same location on a fortnightly basis, using horizontally inserted buriable TDR probes and vertically inserted connector TDR probes. Buriable TDR probes were installed at depths of 5, 10, 15, 20, 30 and 40 cm, providing an average soil moisture measurement over a layer thickness of approximately 4 cm (Soil Moisture Equipment Corp., 1989). The connector TDR probes gave an average soil moisture measurement over depths of 0-5, 0-10, 0-15, 0-20, 0-30 and 0-40 cm, being the length of the probe. The TDR system used was the Soil Moisture Equipment Corporation TRASE TDR, using the standard TRASE calibration to determine the volumetric soil moisture content from the measured dielectric constant. The minimum depths at which the Virrib and buriable TDR probes could be installed without causing a loss of accuracy were 10 cm (Komin, Technical Data) and 5 cm (Soil Moisture Equipment Corp., 1989) respectively. The vertically inserted connector TDR probes were not installed until April 24 1997 and the Campbell CS615 soil moisture sensor was not installed until May 8 1997.

The soil moisture content measurements with the CS615 probe at 5 cm and the Virrib sensor at 10 cm provide the updating observations for the one-dimensional field application, while the Virrib and connector TDR measurements provide data for evaluating the one-dimensional soil moisture profile estimation algorithm. The buriable and connector TDR measurements also provided data for comparison with the Virrib and CS615 measurements. The permanent instrumentation set-up is given in Figure 9.8.

A 1’6” partial flume (Working Group on Small Hydraulic Structures, 1976) was installed at the catchment outlet to monitor surface runoff (Figure 9.9). Discharge was monitored by measuring the water level in a stilling well to the side of the flume, with a water level pressure sensor.

A second pluviometer was located at the flume, and four collecting rain gauges were distributed throughout the catchment to check the spatial variability of rainfall. Collecting raingauges were located at the weather station, flume, and one either side of the catchment at approximately half way between the flume and weather station (Figure 9.4). Collecting raingauges were recorded approximately

a)

b)

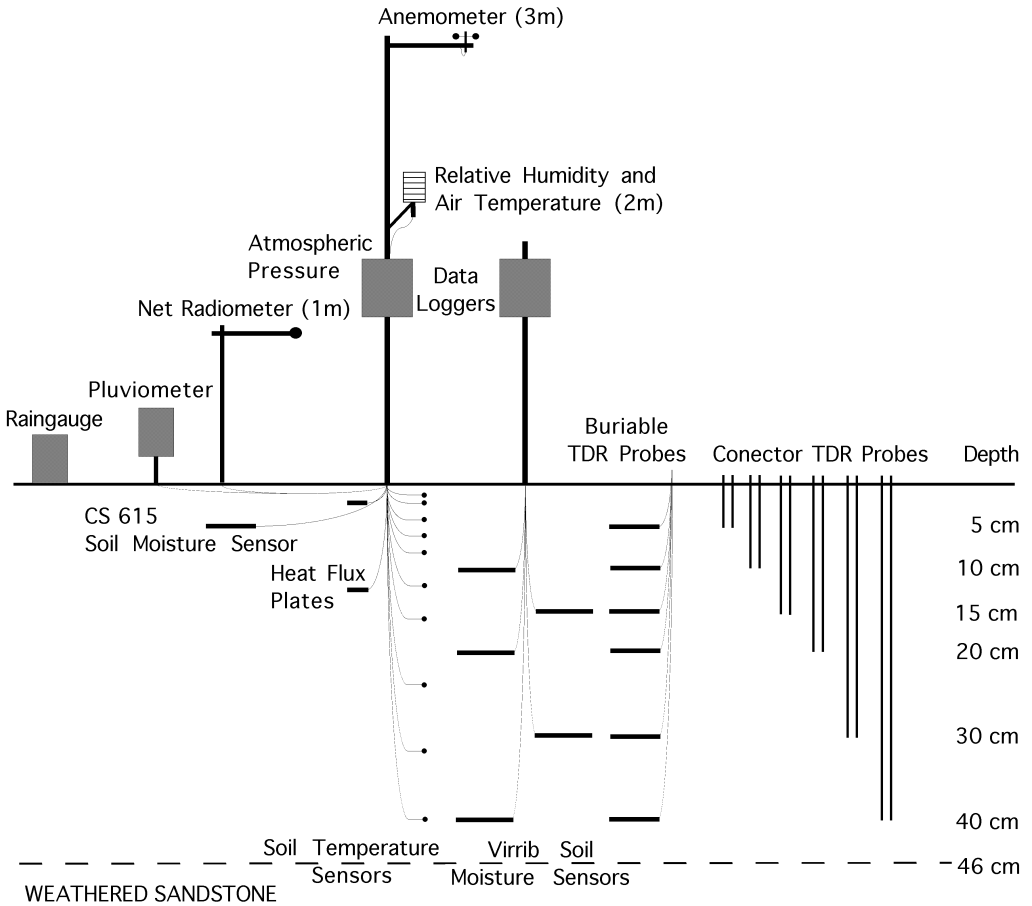

Figure 9.8: Permanent instrumentation set-up: a) photograph; b) diagrammatic illustration.

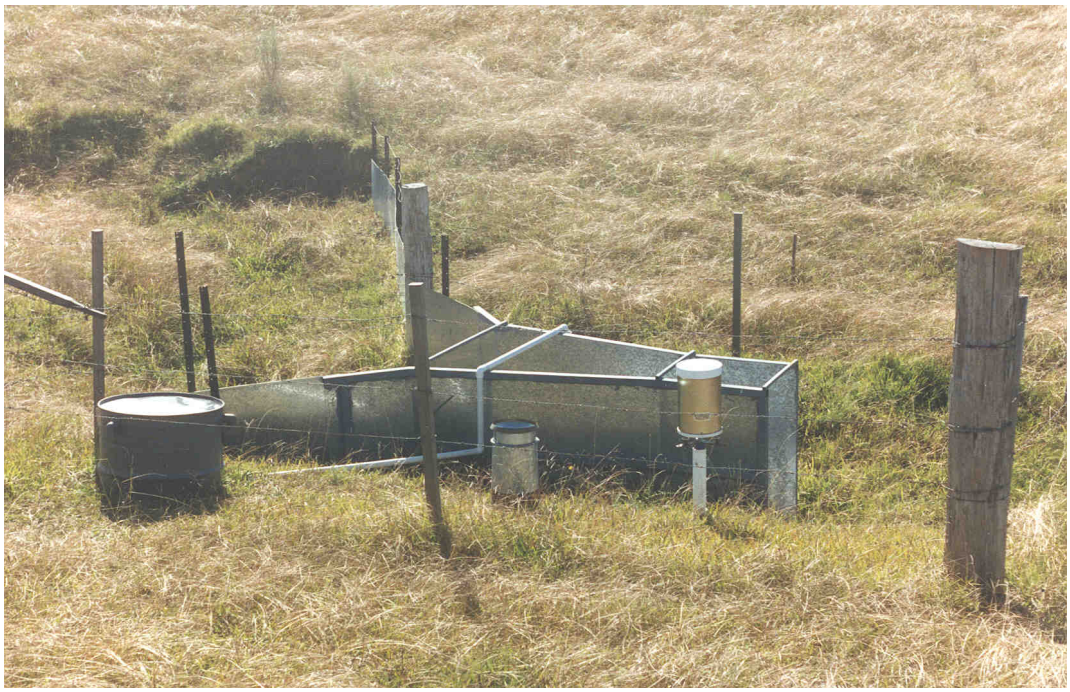

Figure 9.9: Partial flume and raingauges located at the catchment outlet.

fortnightly from December 31 1996. During the intensive field campaign from August 27 1997 to September 22 1997, collecting raingauges were recorded every two to three days.

9.3.1.1 Meteorological Data

The meteorological data collected at the Nerrigundah catchment is given in Appendix B. Figure B.1 is for 1996, Figure B.2 is for 1997 and Figure B.3 is for 1998. Soil heat flux and net radiation data agree with typical values in the literature, with near-surface soil heat flux being approximately 10% of the net all-wave radiation. A decrease in both the soil heat flux and net radiation was observed during winter relative to summer. In addition, periods of lower soil heat flux and net radiation coincided with periods of lower air temperature and periods of rainfall, as a result of cloud cover. Air temperature data agree with expected values, having a range of approximately 10°C to 40°C in summer and approximately 0°C to 20°C in winter.

Atmospheric pressure data indicates a weekly fluctuation superimposed on a yearly cycle, going from a minima around February where maximum rainfall was received, to a maxima around July where minimum rainfall was received. The data also shows that localised low pressures correspond with periods of rainfall.

9.3.1.1.1 Precipitation

To compare the two pluviometers in the catchment, double mass curves for the periods of continuous data in 1997 and 1998 were generated (Figure 9.10). The double mass curve clearly demonstrates that there was a small (less than 5%) systematic difference between the two raingauges, with the pluviometer located at the flume having systematically recorded more rainfall than the pluviometer at the weather station. It is unlikely that this was a result of spatial variation in rainfall, but rather because the pluviometer at the weather station was more exposed than that at the flume, resulting in more rainfall being blown past the pluviometer.

As a further check on the pluviometers and rainfall variability within the catchment, comparisons were made between the collecting raingauges and the pluviometers (Figure 9.11 and Figure 9.12). This comparison shows that there was less than 14% difference between collecting raingauges, and between pluviometers and collecting raingauges. The conclusion drawn from this was that negligible spatial variation of rainfall occurred across the Nerrigundah catchment.

The only dates for which there was any obvious trend in the comparison of collecting raingauge data were April 28, May 7 and May 21 1998. However, the trend was not such that it would suggest the catchment was on the edge of a rainfall event, but rather a variation of rainfall within the rainfall event, with raingauges at the top and bottom of the catchment receiving more rainfall than those located midway.

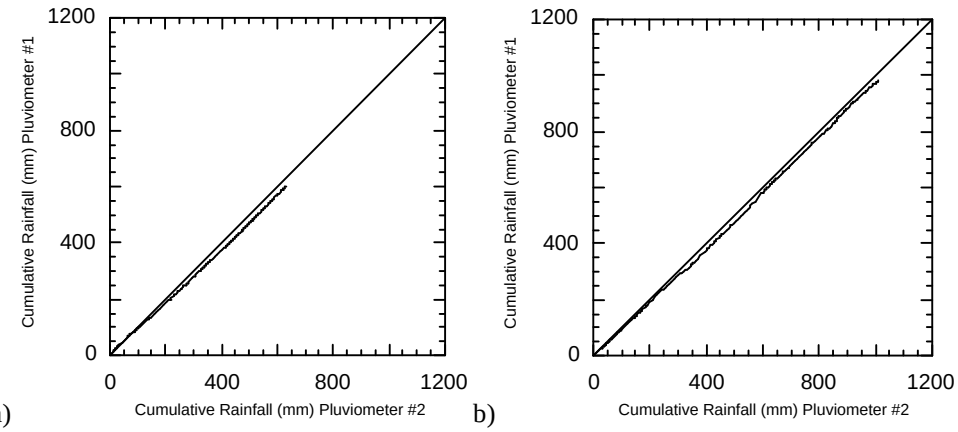

Figure 9.10: Double mass curve for the two pluviometers located in the Nerrigundah catchment: a) Julian day 38 to 325 1997; and b) Julian day 1 to 290 1998.

The collecting raingauge data was only recorded approximately once every two weeks, so there was evaporation from the collecting raingauges during the summer months. However, all four collecting raingauges should be affected equally, allowing conclusions to be reached regarding the spatial variation in rainfall across the catchment.

The comparison of collecting raingauges with both pluviometers indicates periods where there was obvious evaporation from the raingauges. These periods were mostly during the summer months. Examples of this are February 14 and October 14 1997 in Figure 9.11a and Figure 9.11b, and January 22 to April 1 1998 in Figure 9.12a and Figure 9.12b.

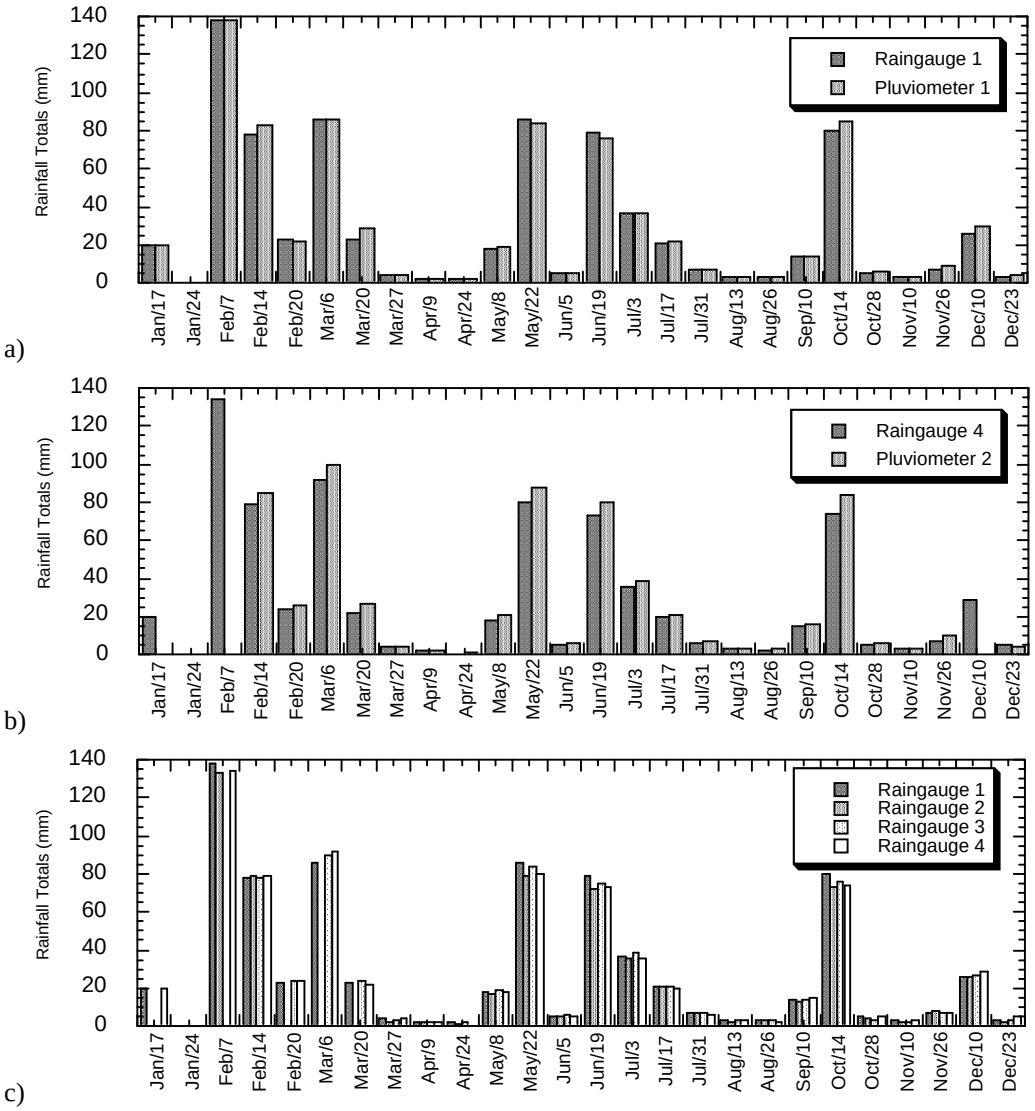

Figure 9.11: Comparison of collecting raingauge data with pluviometer data for 1997.

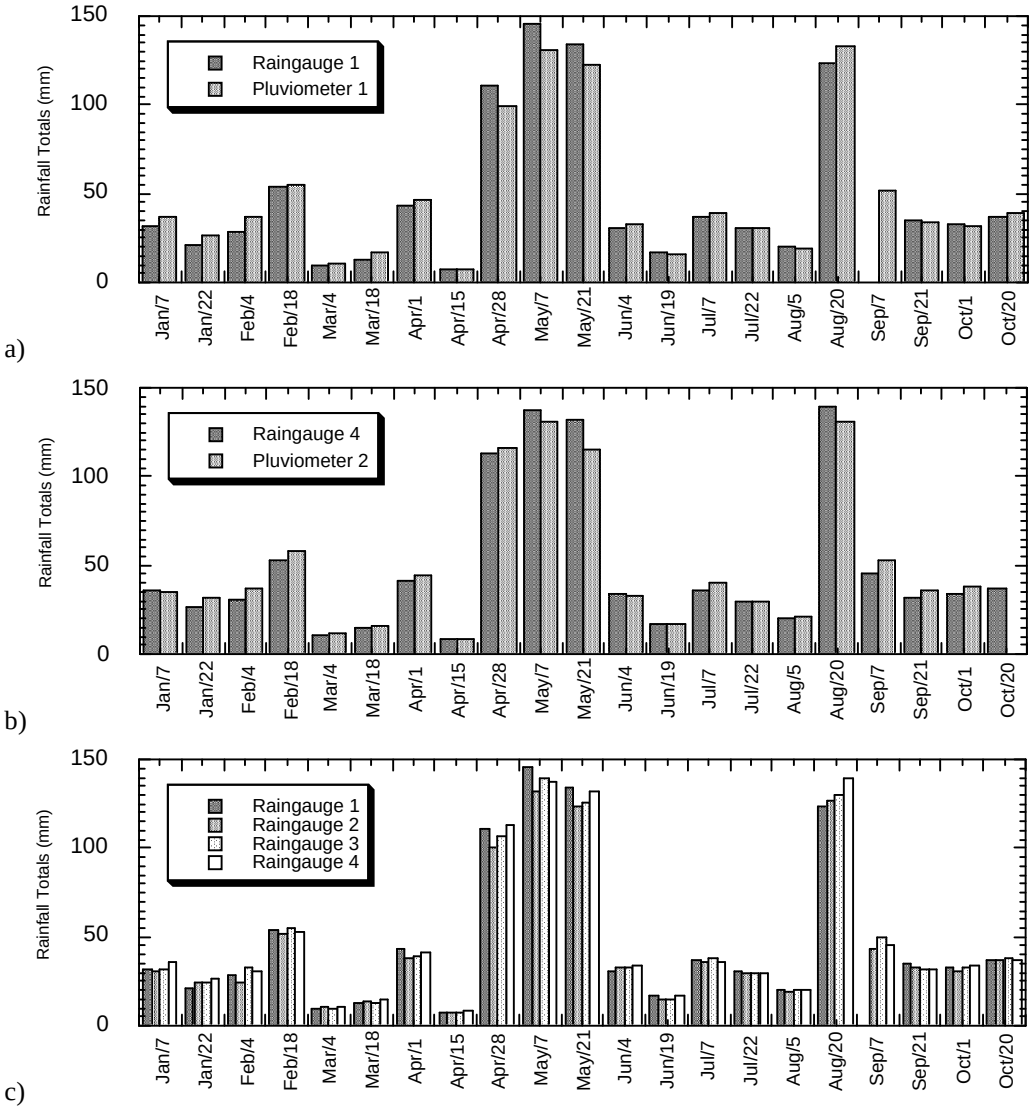

Figure 9.12: Comparison of collecting raingauge data with the pluviometer data for 1998.

Collecting raingauge observations which exceed the pluviometer data are indicative of periods where the rainfall rate exceeded the maximum rainfall rate that the tipping bucket raingauge could accurately measure. Examples of this are May 22 and June 19 1997 in Figure 9.11a. However, Figure 9.11b shows the reverse trend, indicating that this was not the case. Another example of this reverse trend is August 20 1998. There are however three dates which provide consistent data to indicate periods of high rainfall intensity. These dates are April 28, May 7 and May 21 1998.

9.3.1.1.2 Soil Temperature Profile

The temporal variation of the soil temperature profile is given in Figures B.1 to B.3 in Appendix B. The white strip along the top of Figure B.2p and Figure B.3p correspond with the soil temperature sensor at 0.5 cm being damaged during installation of the Campbell CS615 soil moisture sensor on Julian day 128 1997. A comparison of the soil temperature measurements at 40 cm depth with those at 1 cm depth is also given in Figure B.1 to Figure B.3. Coincidently, on Julian day 129 1997 (Figure B.2k) there was a sudden drop in the near-surface soil temperature, which was followed by the temperature measurements at 40 cm depth a few days later. The decrease in soil temperature throughout the entire soil profile is seen clearly in Figure B.2p. This rapid decline in soil temperature was the result of a decrease in air temperature at the onset of a rainfall event that saturated the soil profile (see Figure B.2q). This type of response is seen again on Julian day 112 1998 (Figure B.3).

Whilst the sudden decline in soil temperature on Julian day 129 1997 could be readily explained by the sudden decrease in air temperature, this did not explain the accompanying increase in diurnal variation of soil temperature at 1 cm depth, which would be expected to also decrease. As this increase in diurnal variation coincided with a major wetting event, it was thought that soil might have been eroded from above the soil temperature sensor, exposing it to direct sunlight. To further investigate this, comparisons of soil temperature observations at increasing depths were made with the soil temperature observations at 40 cm. These comparisons are given in Figure B.4 for 1997 and Figure B.5 for 1998.

These plots show that from Julian day 129 1997 there was an increase in the diurnal variation of soil temperature for all depths, with this being consistent through into 1998. This increase in diurnal variation is also apparent in Figure B.2p and Figure B.3p.

In addition to the direct comparisons, double “mass” curves of daily average soil temperature were generated, to investigate “changes” in soil temperature measurement. The double mass curves in Figure 9.13 show that for the beginning of 1997 there was a 1:1 relationship between the soil temperatures at 40 cm and at all other depths. However, after Julian day 145 1997 (cumulative

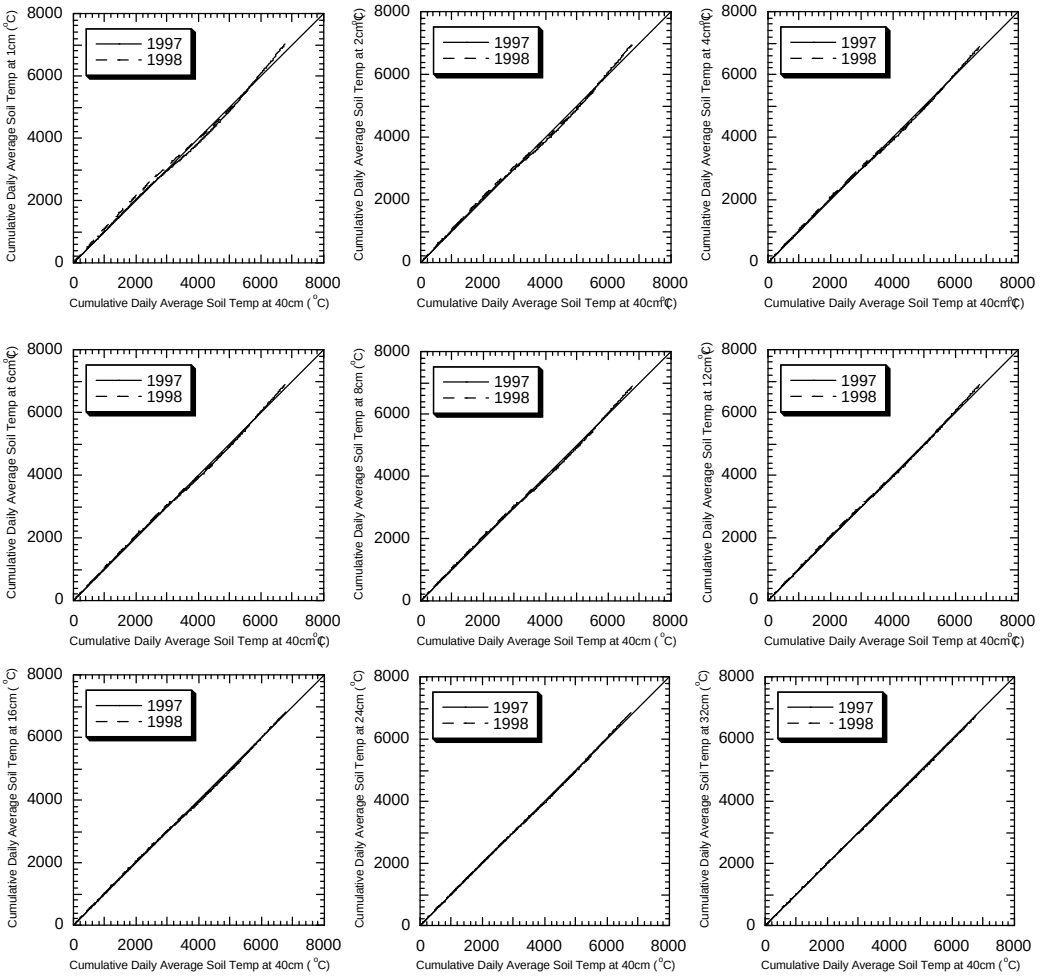

Figure 9.13: Double "mass" curves of soil temperature for various depths.

daily soil temp of 3000°C) the cumulative soil temperature at 40 cm depth began to increase relative to shallower depths. This was followed by a decrease in the cumulative soil temperature at 40 cm relative to shallower depths. This sinusoidal pattern agrees with intuition, as soil temperature is greater at depth during winter when there is a net cooling of the soil profile and greater at the soil surface during summer when there is a net warming of the soil profile. Although the magnitude of this seasonal trend decreased with depth, it was consistent throughout the entire profile. This indicates that up until Julian day 145 1997, the soil temperature sensors were not responding correctly to changes in soil temperature. The graph for 1998 shows the same seasonal trend as for 1997, but without the straight line section at the start of the year.

Whilst the comparisons of soil temperature for various depths in Figure B.4 and Figure B.5 confirm that the soil temperature sensor at 1 cm depth

was not exposed to direct sunlight, the double "mass" curves in Figure 9.13 indicate that prior to the major wetting event on Julian day 129 in 1997, the soil temperature sensors were not responding correctly to changes in soil temperature. This was most likely a result of the sensors being installed under dry conditions, resulting in poor contact between the temperature sensors and the soil. Hence, the diurnal variation of soil temperature seen in the observations prior to Julian day 129 1997 were most likely due to the variation in temperature of entrapped air surrounding the soil temperature sensor. This highlights the difficulties associated with installing monitoring equipment in "undisturbed" soil and the importance of leaving monitoring equipment in place for relatively long periods of time. In this instance, three major infiltration events were required before the temperature sensors began operating correctly.

9.3.1.1.3 Soil Moisture Profile

The Virrib soil moisture sensors consist of two stainless steel concentric circular rings (electrodes of diameters 28 cm and 20 cm, Figure 9.14a). Measurements of soil moisture content using the Virrib sensors are made by means of an electro-magnetic wave between these two electrodes. The sensor produces an output between 5 and 55 mA, which corresponds to a soil moisture content range from 5 to 55% v/v. Soil moisture measurements using the Virrib sensors are reported to be independent of the soil chemical properties. Therefore the device does not have to be calibrated, and its precision remains unaffected by long term use and application of chemical fertilisers. Due to the diameter of the outer electrode and the layer thickness over which the sensor output responds (12 cm), the sensor provides average soil moisture measurements for a 20 litre volume of soil (Komin, Technical Data).

The Campbell CS615 water content reflectometer consists of two 30 cm long stainless steel probes connected to a printed circuit board (Figure 9.14b), and measures the soil moisture content using the TDR technique. The CS615 reflectometer is specified to have an accuracy of ±2.5% v/v when applied to typical mineral soils using the manufacturers standard calibration relationship. Soils with different dielectric properties are reported to show an error that will appear as a constant offset. However, both the accuracy and stability of the sensor

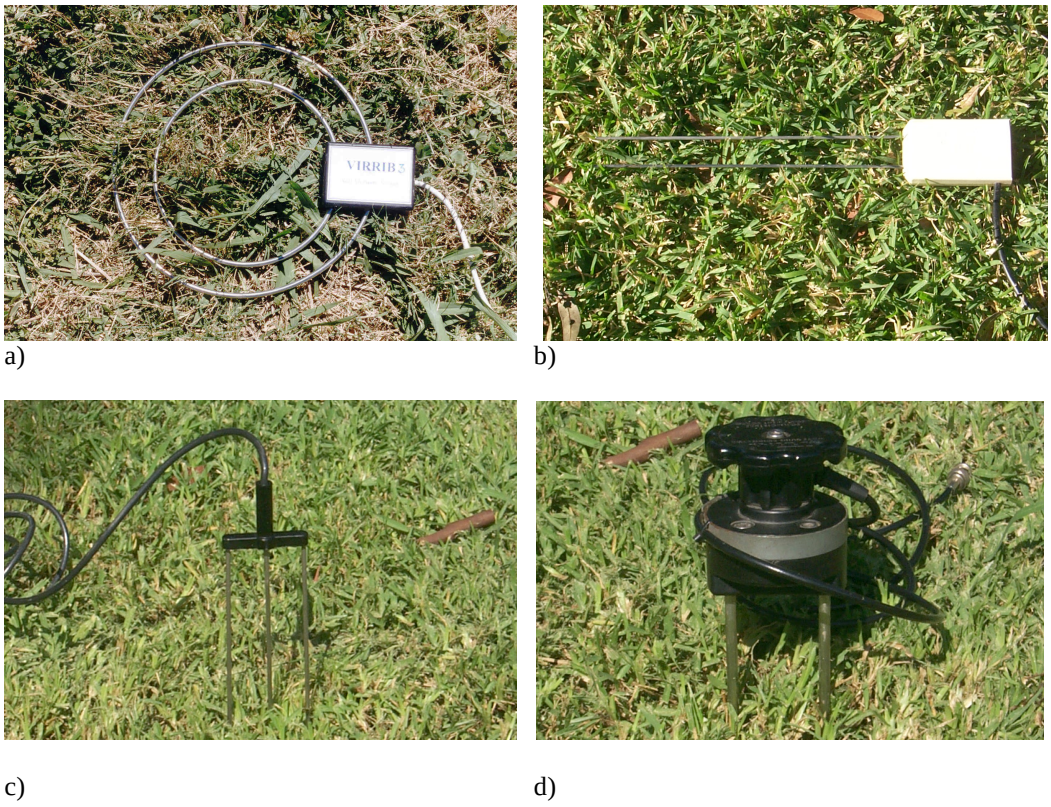

Figure 9.14: a) Virrib soil moisture sensor; b) CS615 reflectometer soil moisture sensor; c) Buriable TDR soil moisture sensor; and d) Connector TDR soil moisture sensor.

are affected by the soils electrical conductivity. With soil electrical conductivity above 2 dSm^{-1} the probe output is reported to change and at electrical conductivity values greater than 20 dSm^{-1} the probe output is reported to become unstable. An important consideration with the CS615 reflectometer is its strong dependence on soil temperature. To account for this temperature dependence, a temperature correction polynomial has been supplied (Campbell Scientific Inc., 1995).

The buriable TDR sensors (Figure 9.14c) consist of three 20 cm probes, whilst the connector TDR sensors (Figure 9.14d) consist of two stainless steel probes of user specified length and a balun. These sensors were measured using the TRASE TDR system, specified to have an accuracy of ±2.5% v/v when applied to typical mineral soils using the manufacturers standard calibration relationship (Soil Moisture Equipment Corp., 1989).

Given the design of the Virrib sensors, installation required excavation and recompaction of the soil in which the sensors were placed for measurement of soil moisture content. To minimise the effects of soil disturbance, the soil was

replaced in the same order from which it was removed, with as little soil mixing as possible. Due to the disturbance of the soil, these sensors are reported to generally require a few months settling in time before representative soil moisture measurements may be made (Komin, Technical Data).

As the CS615 reflectometer and buriable TDR soil moisture sensors consist of probes, these sensors could be inserted into undisturbed soil from the side of the excavation. Therefore, measurements made using these sensors should not be affected by disturbance to the soil from excavation to the same extent as the Virrib sensors. However, the disturbance caused by the actual insertion of the probe into the soil may be significant for larger probe diameters. Rothe *et al.* (1997) have shown that merely pushing the TDR probes into the soil entails a reduction of the measured soil moisture content of up to 10% v/v, with the effects being strongest close to saturation. Therefore, for probe diameters greater than 6 mm, Rothe *et al.* (1997) suggest that it is necessary to remove soil in advance to probe installation by drilling.

Buriable TDR sensors have a probe diameter of 3.2 mm. However, due to the dry state of the soil at time of installation, the soil was extremely hard and installation was difficult, requiring holes to be formed prior to installation of the sensors. Thus the buriable TDR sensors could be prone to suffer from air gaps. CS615 reflectometer sensors also have a probe diameter of 3.2 mm, but due to the moist state of the soil at time of installation, the sensor could be easily installed without pre-forming holes. The connector TDR sensors consist of two 6 mm diameter probes that are inserted from the soil surface. Given the design and diameter of these probes, they could be inserted from the surface without causing air gaps, even under dry soil conditions.

The horizontal layout of soil moisture sensors is shown in Figure 9.15. To prevent opportunistic flow along sensor leads, sensor leads were brought to the surface via PVC conduit. Leads were fed through a hole in the side of the PVC conduit and sealed with silastic, and bentonite placed around the PVC conduit to prevent opportunistic flow down the sides of the PVC conduit.

There are upper and lower limitations on the length of connector TDR probes that may be used. The upper limit on probe length is governed by the

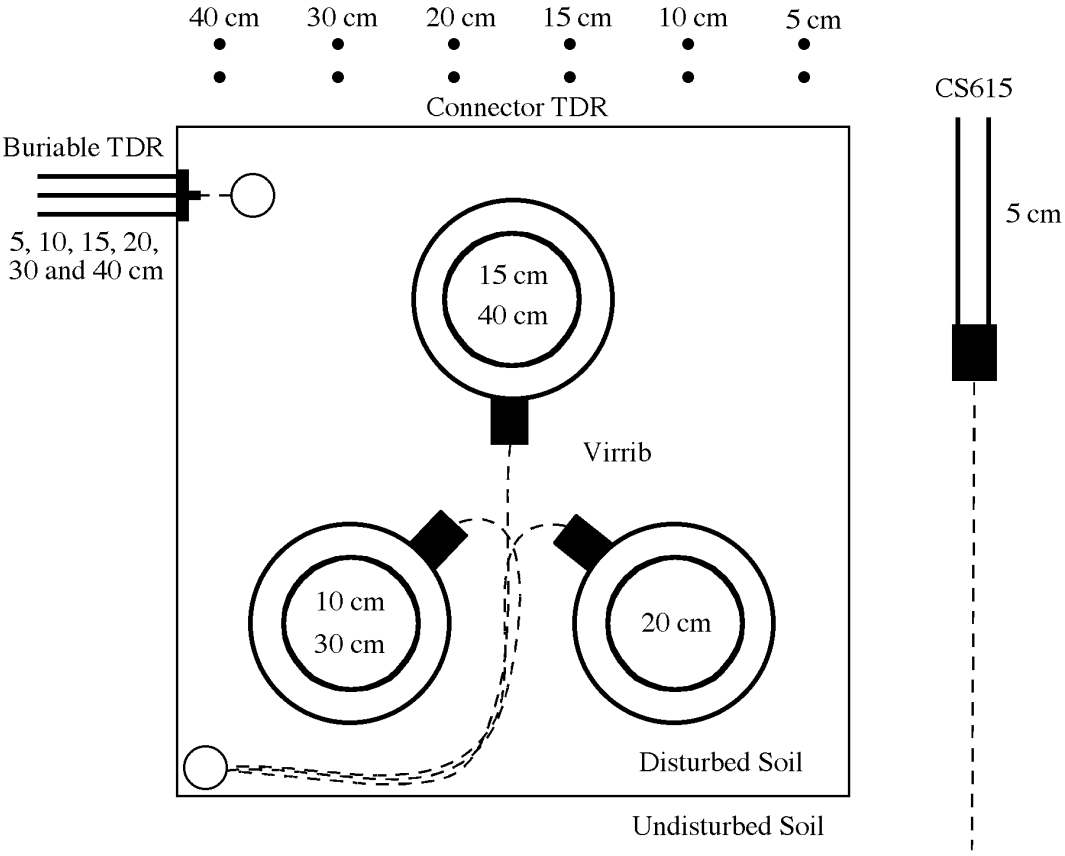

Figure 9.15: Horizontal layout of the soil moisture sensors for measurement depths/probe lengths indicated.

strength of arm of the person who inserts the probe. However, a more severe limit to probe length arises from loss of TDR signal in the soil (Zegelin, 1996). To overcome the strength of arm limitations, connector TDR probes of greater than 15 cm length were inserted by hammering in conjunction with probe insertion guides, as shown in Figure 9.16.

The lower limit on TDR probe length is imposed by the accuracy of the time-of-travel measurement of the TDR device, which is currently of order 0.1 ns, limiting probes to greater than 5 cm (Zegelin, 1996). However, Zegelin (1996) has noted that probe lengths of 10 cm even have a reduced accuracy because of this timing limit, and Soil Moisture Equipment Corp. (1989) warn against using connector TDR probe lengths of less than 15 cm due to a loss of accuracy. Therefore, calibration of the connector TDR probes of length 5, 10 and 15 cm was evaluated from thermogravimetric samples taken from various locations in the Nerrigundah catchment. The calibration of longer TDR probes was not evaluated due to the destructive nature and labour intensiveness of the testing, and the

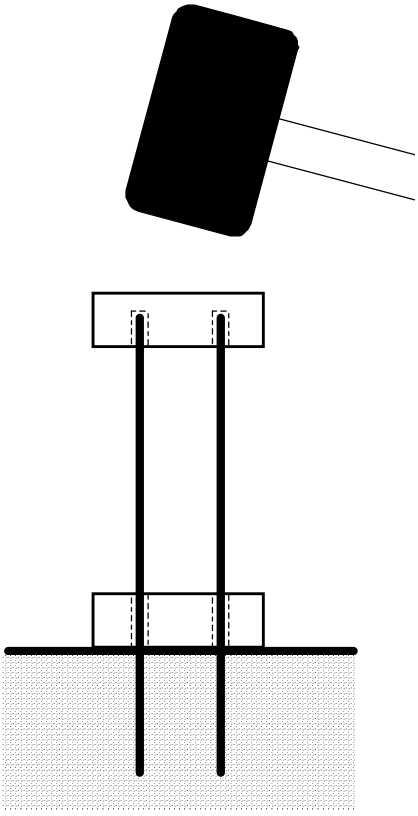

Figure 9.16: Insertion of long connector TDR probes.

number of calibration data values required to make conclusive statements regarding accuracy. In addition, literature suggests that longer probes should not result in any further loss of accuracy. Hence, providing satisfactory calibration results were obtained for the shorter probes, measurements made with longer probes should also be of sufficient accuracy.

The calibration of connector TDR probes was achieved by firstly clearing a small patch of soil from grass vegetation. Soil moisture measurements were made using the 5, 10 and 15 cm connector TDR probes in exactly the same location. A 10 cm diameter soil sampling ring of 5 cm depth was then placed over the area of soil in which the soil moisture measurements were made. Three consecutive soil samples were taken, such that a 15 cm depth sample of soil was retrieved. The samples were then weighed both before and after oven drying. Subsequently, soil density and in-situ thermogravimetric soil moisture content for the three probe lengths was determined.

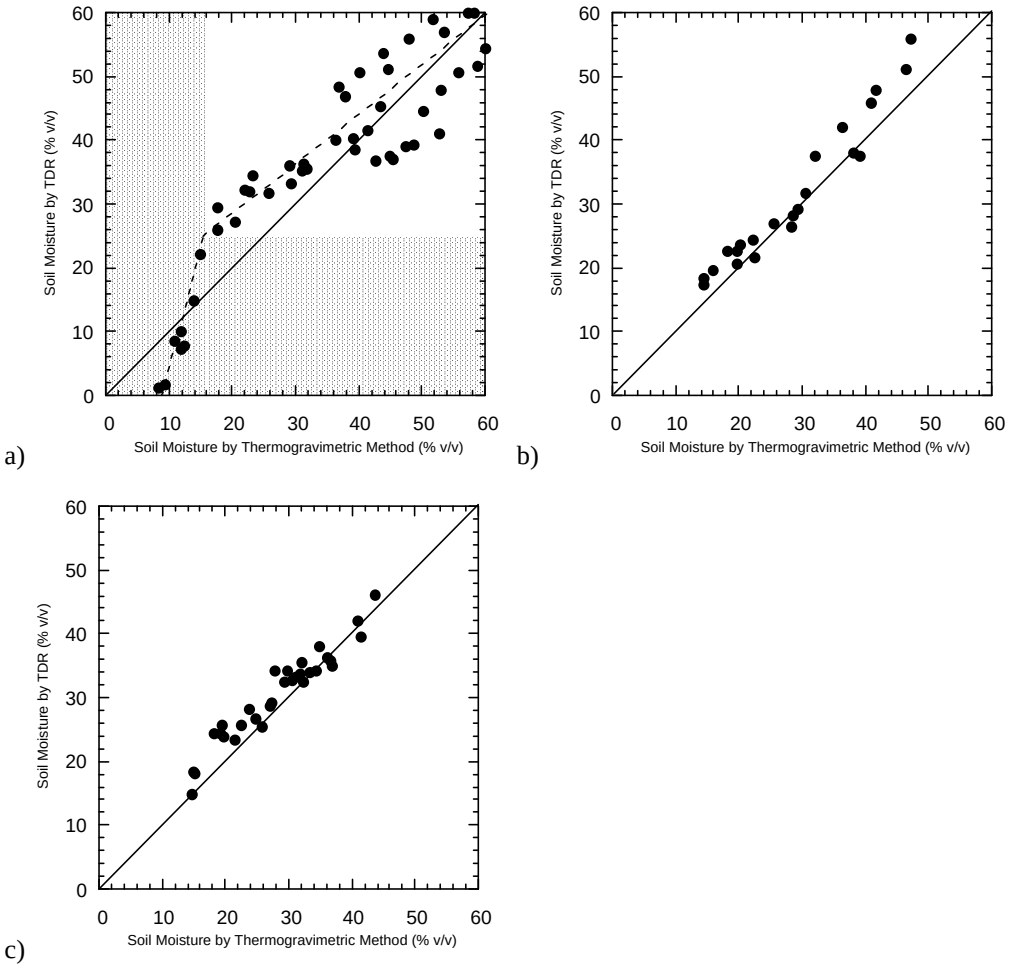

Figure 9.17: Comparison of thermogravimetric and connector TDR soil moisture measurements for varying probe lengths: a) 5 cm; b) 10 cm; and c) 15 cm.

The results from calibration of connector TDR probes are given in Figure 9.17, where it can be seen that 10 and 15 cm probes have a near linear 1:1 relationship with approximately the ±2.5% v/v accuracy stated by the manufacturer. However, results from the calibration of 5 cm probes may be interpreted in three different ways:

i) TDR soil moisture measurements follow a 1:1 relationship with the thermogravimetric samples but have a very low accuracy, approximately ±7% v/v. This interpretation requires the assumption that the lack of spread around the 1:1 line at soil moisture contents below 40% v/v is due to an insufficiently large sample size.

ii) There is a non-linear or non-continuous relationship between TDR soil moisture measurements and the thermogravimetric observations. Using this

interpretation, individual relationships may be fitted to TDR soil moisture observations above 25% v/v and TDR soil moisture observations below 25% v/v.

iii) For soil moisture content less than 15% v/v the TDR method cannot measure soil moisture content reliably using 5 cm probes, with a variation of 20% v/v from the TDR for essentially the same thermogravimetric soil moisture content.

A reason for (iii) may be that as soil becomes drier, the dielectric constant of the soil is reduced, and hence the velocity of the electromagnetic wave increases. The effect of this increase in velocity would be to make determination of the travel time along the wave guide more difficult due to the shortness of the wave guide. Timing errors will also have a greater influence on the soil moisture content extracted from shorter probes. From this third interpretation, a linear relationship may be fitted to TDR observations above 25% v/v, and any TDR soil moisture observations below 25% v/v regarded as erroneous. In application of the 5 cm TDR soil moisture observations, data was used as measured, with the assumption of a low accuracy.

Soil moisture profile data in Figure B.1 to Figure B.3 show a rapid wetting up of the soil in response to rainfall, followed by a much slower drying out of the soil in response to evapotranspiration. The data also shows that deeper soil layers were generally wetter than near-surface soil layers and that the near-surface soil layer was more dynamic in response to surface fluxes. Furthermore, the CS615 sensor yields soil moisture data as high as 70% v/v in the near-surface soil layer, whilst the Virrib sensor yields soil moisture data only as high as 46% v/v. The maximum soil moisture content of 46% v/v from the Virrib sensor at 10 cm depth agrees with the undisturbed soil porosity measured in the field (see Table B.5). However, a maximum soil moisture content of 50% v/v from the Virrib sensor at 40 cm depth and 70% v/v for the CS615 at 5 cm depth do not agree with the undisturbed soil porosities of 32% v/v and 52% v/v respectively. Whilst the discrepancy with the Virrib sensor may be explained by the recompaction of soil during installation, the discrepancy with the CS615 is more difficult to explain. The Virrib soil moisture sensors show more noise in the soil moisture

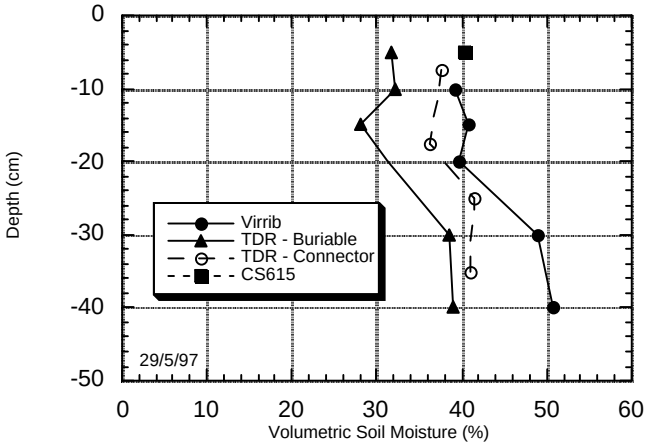

Figure 9.18: Comparison of Virrib, connector TDR, buriable TDR and CS615 reflectometer soil moisture measurements.

measurement than the CS615 sensor and the CS615 sensor indicates a diurnal variation in soil moisture content, which may be a result of the soil temperature correction.

An in-situ calibration of the soil moisture sensors installed at the weather station could not be performed without destroying the soil moisture monitoring site. Hence, evaluation of soil moisture measurements was performed by making comparisons between the different soil moisture sensor types, and using the calibration of connector TDR probes to give confidence in the connector TDR soil moisture measurements.

A selection of soil moisture profile measurements from the Virrib, connector TDR, buriable TDR and CS615 reflectometer soil moisture sensors are compared in Figure B.6. An example of this data is given in Figure 9.18. These comparisons show that the Virrib sensors continually gave soil moisture measurements approximately 10% v/v higher than the buriable TDR sensors. Plotting of the soil moisture profile measurements at discrete times also revealed that the soil moisture measurements did not indicate a smooth variation of soil moisture content with depth. This may be a result of: (i) inaccurate measurement of soil moisture content by the sensors; or (ii) physical differences in soil moisture content with depth as a result of natural variation in soil properties, which is most likely to be the case.

In addition to making comparisons of soil moisture profiles at discrete times, continuous time comparisons are made for discrete layers in Figure B.7.

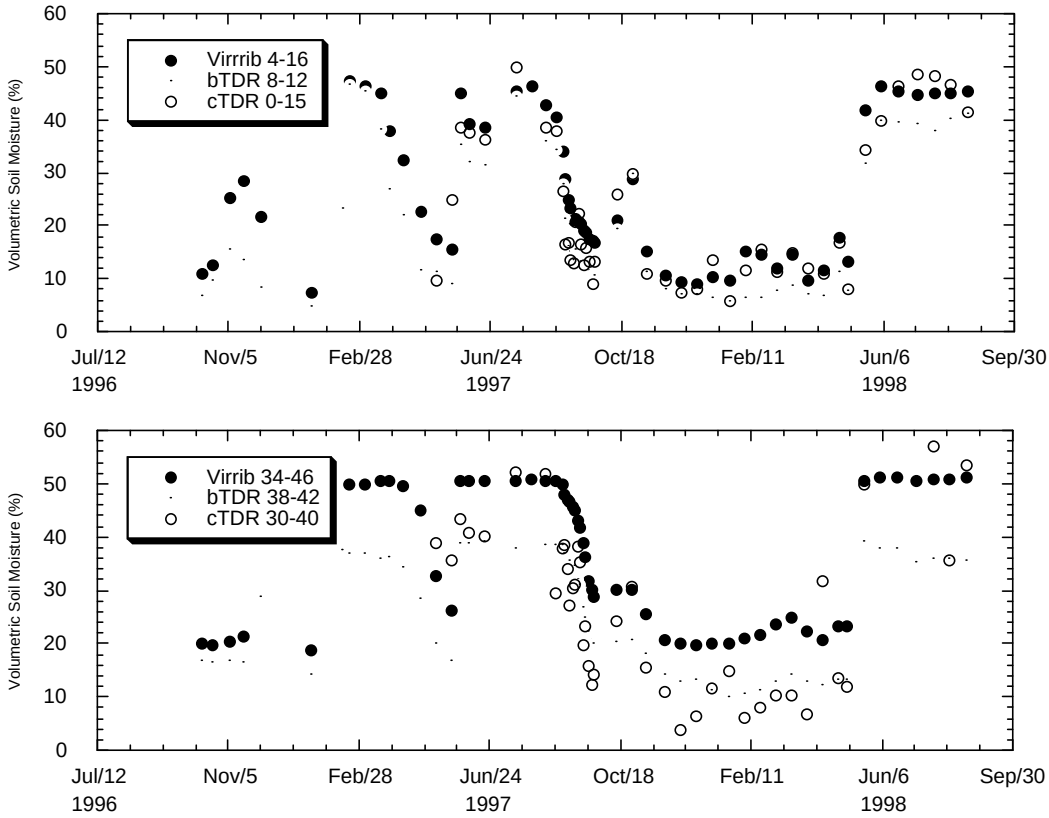

Figure 9.19: Comparisons of soil moisture measurements for Virrib, buriable TDR and connector TDR, for soil layer depths indicated (cm).

Figure 9.19 shows examples of the soil moisture time series for soil moisture measurements near the soil surface and at depth. These plots show that while there is generally a good agreement between the connector TDR and Virrib measurements for the top 15 cm of the soil profile, comparisons between the connector TDR measurements and the other sensors are qualitatively worse for deeper layers.

The poor comparison between connector TDR, buriable TDR and Virrib soil moisture measurements for layers other than the top 15 cm indicated that aggregation of the Virrib and buriable TDR measurements throughout the profile may yield better comparisons with the connector TDR than for the disaggregation of connector TDR measurements. This is because small differences in soil moisture measurements for the connector TDR probes can yield large differences in layer estimates of soil moisture content when performing the disaggregation.

Comparisons of soil moisture using the aggregated observations are given in Figure B.8, with an example of these comparisons given in Figure 9.20 for a

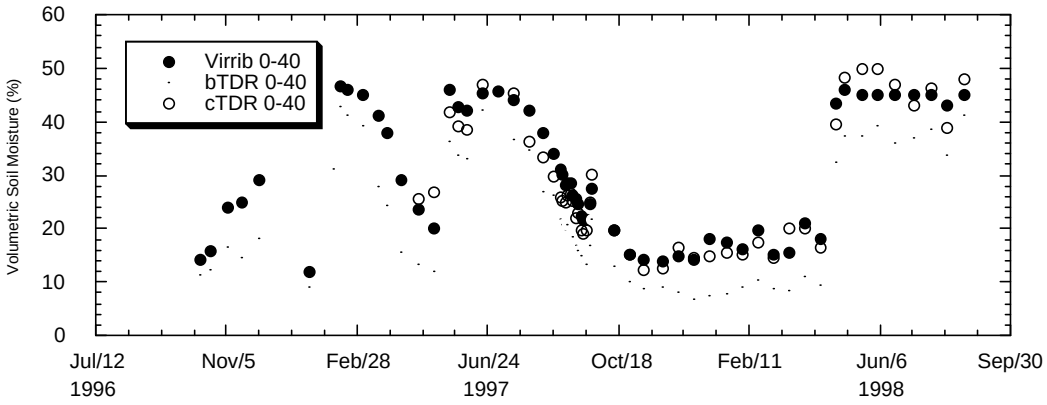

Figure 9.20: Comparison of soil moisture measurements for Virrib, buriable TDR and connector TDR, to a soil depth of 40 cm.

soil profile depth of 40 cm. The results from comparisons using the aggregated observations indicated a generally good agreement between the Virrib and connector TDR for all depths. However, the poor comparison with buriable TDR was still apparent.

Immediately following periods of infiltration (February 14 1997, May 22 1997 and April 28 1998), the Virrib sensors appeared to systematically suggest greater soil moisture content than both the buriable TDR and connector TDR soil moisture measurements (Figure 9.20). To identify if the Virrib sensors were over-responding to the addition of soil moisture content or if the TDR sensors were under-responding to the addition of soil moisture content, a comparison of cumulative change in soil moisture storage based on the soil moisture measurements was made with a simple bucket water balance model (Figure 9.21).

In the water balance model, it was assumed there was no flux from the bottom of the soil profile, all rainfall infiltrated up to the maximum soil moisture storage, and evapotranspiration was estimated from the Penman-Monteith potential evapotranspiration (section 9.4.1.2), reduced by a soil moisture stress index (section 9.4.1). Soil moisture storage calculations were commenced from installation of connector TDR probes (April 24 1997), and were normalised so that soil moisture storage estimates were the same for each sensor type at commencement of calculations. The results from this analysis indicate that the Virrib sensors were over-responding to the addition of soil moisture content, with connector TDR soil moisture measurements and water balance calculations having a good agreement for the two major infiltration events shown in this data.

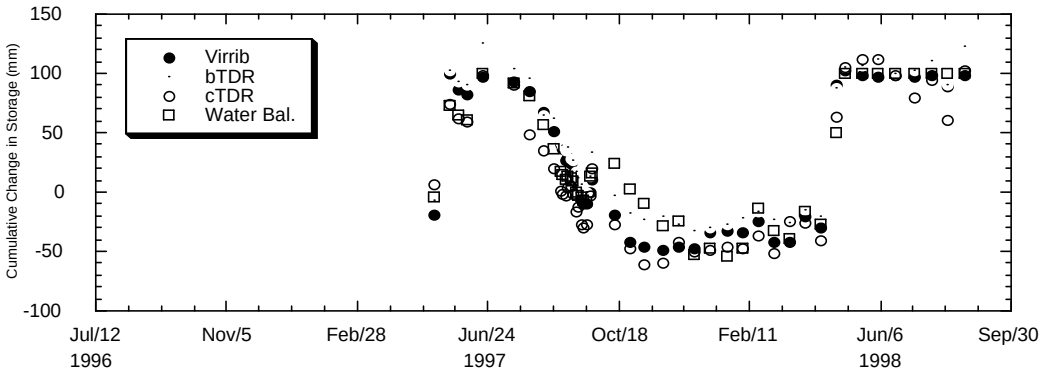

Figure 9.21: Comparison of cumulative change in soil moisture profile storage for Virrib, buriable TDR, connector TDR and a bucket water balance model.

The other discrepancy between connector TDR and Virrib soil moisture measurements (Figure 9.20) was the dry down period from July 1997 to October 1997. During this period, the Virrib sensor data shows a consistently wetter estimate of the soil moisture content. The comparison with water balance calculations again showed favour with the connector TDR measurements. The large discrepancy of water balance calculations with measurements from October 1997 to January 1998 was a result of the model assuming that all rainfall infiltrated. At lower soil moisture contents and for heavy rainfall this is not the case, with infiltration capacities being less than the rainfall rate.

Although Figure 9.21 showed a reasonably good agreement between the connector TDR measurements and water balance calculations, there was still some concern about the consistently large difference between the buriable TDR measurements and those from the other sensors. Therefore, an investigation into the variability of soil moisture content over reasonably short length scales was undertaken to see if the differences in the soil moisture measurements were due to actual differences in soil moisture as a result of natural variation in soil properties.

For this investigation, a transect of soil moisture measurements was made with the 15 cm connector TDR probes every 0.5 m for a distance of 25 m, under both saturated and somewhat drier conditions. The measurements made under drier conditions were also made in two perpendicular directions. Measurements were made in an approximately level area near the permanent instrumentation in the top of the catchment, to minimise any effects from lateral redistribution. The variogram and autocorrelation function for each of these sets of soil moisture measurements was determined (Figure 9.22 and Figure 9.23).

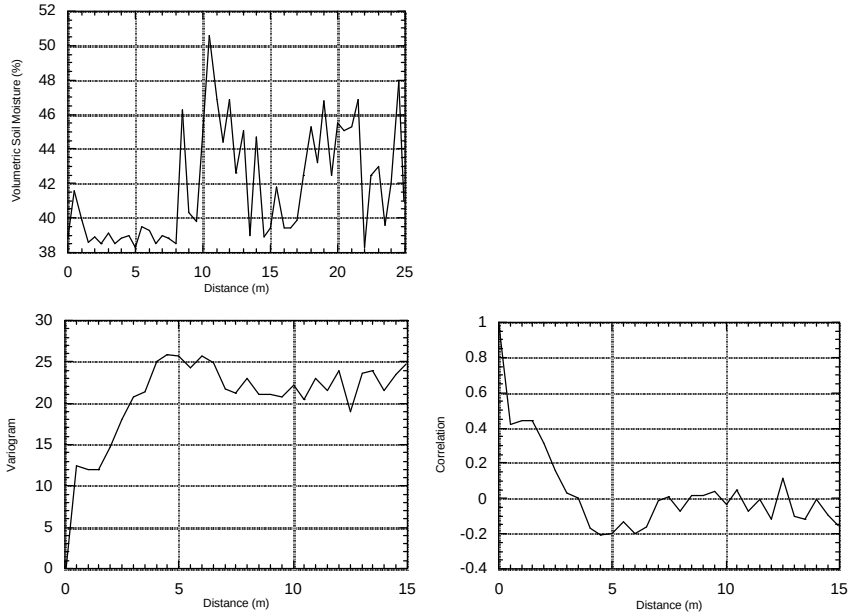

Figure 9.22: Transect soil moisture measurements, autocorrelation, and variogram for 25 m transect on 19/6/97.

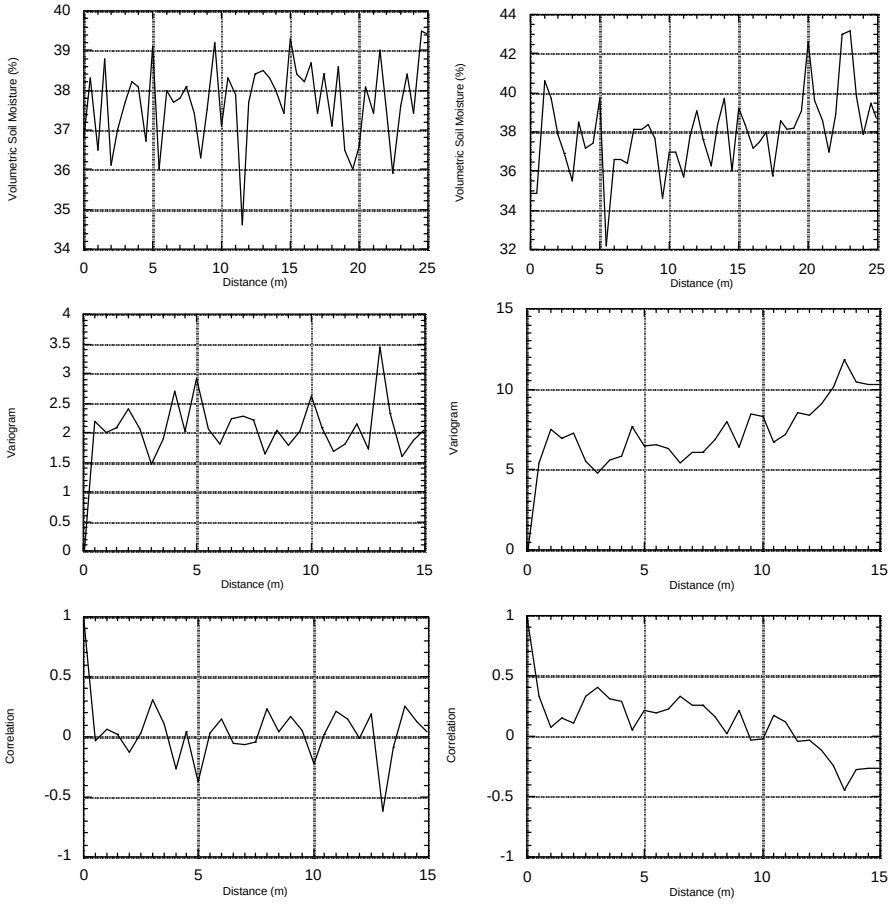

a) b)

Figure 9.23: Transect soil moisture measurements, autocorrelation, and variogram for 25 m transect on 17/7/97. a) Down slope; and b) across slope.

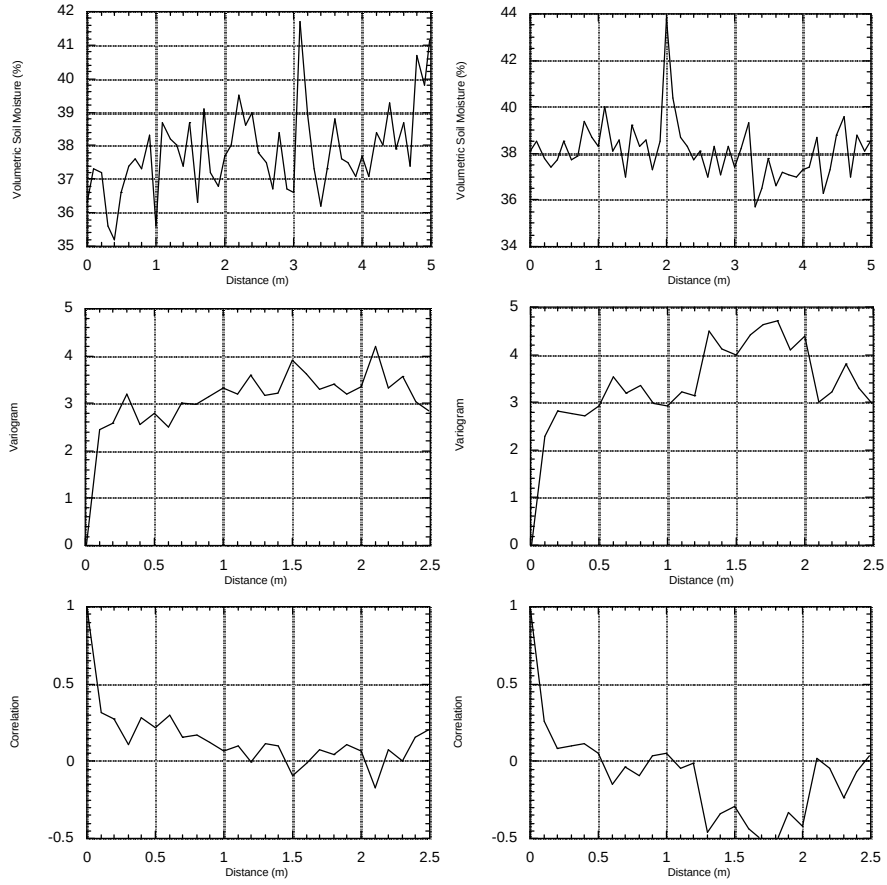

Figure 9.24: Transect soil moisture measurements, autocorrelation, and variogram for 5 m transect on 18/7/97. a) Down slope; and b) across slope.

Due to the saturated condition of the soil, the measurements on June 19 1997 reflect the variation in soil porosity, whilst the measurements on July 17 1997 reflect the variation in soil moisture content due to variations in soil properties such as soil texture, and noise in the TDR measurement technique. Both of the figures indicate a very short correlation length, with the variogram suggesting a nugget effect due to error in the TDR measurement technique of between 1 and 3% v/v.

As no autocorrelation could be seen at a measurement spacing of 0.5 m, the measurements were repeated for a measurement spacing of 0.1 m. The results given in Figure 9.24 again indicate a very short correlation length, with the variogram suggesting a nugget effect due to error in the TDR measurement technique of approximately 1.5% v/v.

As the difference in soil moisture measurements could not be explained by a short scale natural variation in the soil properties, an alternative explanation was sought. The installation procedure for the Virrib sensors was considered to still be a contributing factor to the differences in soil moisture content. Therefore, measurements were made using 15 cm and 30 cm connector TDR probe lengths in the disturbed soil where the Virrib sensors were installed, and in the undisturbed soil in the locality of the buriable TDR sensors. On July 31 1997, the average soil moisture measurements in the disturbed soil were 38.2% v/v and 37.4% v/v for the 15 cm and 30 cm probe lengths respectively, whilst the average soil moisture measurements in the undisturbed soil were 35.9% v/v and 35.6% v/v for the 15 cm and 30 cm probe lengths respectively. Soil moisture measurements were approximately 2% v/v drier in the undisturbed soil in both instances.

The conclusion drawn from these observations was that the differences in the soil moisture measurements from the different sensors were the result of a combination of factors. Firstly, the installation procedure for the Virrib sensors involved major disturbance to the soil in which soil moisture was being measured, thus altering the physical properties of the soil, and still influencing the physical moisture content of the soil in comparison to the undisturbed soil even after 9 months. Secondly, the different sensors use different measurement techniques and measure the soil moisture of different size volumes of soil. Thirdly, any air gaps or fluid filled gaps around the TDR probes due to insertion affect the ability of the TDR technique to measure the moisture content of the soil accurately (Knight *et al.*, 1997). The effect of gaps is reported to be greater for three-rod probes (ie. buriable TDR) than two-rod probes (ie. connector TDR and CS615), and if the gaps are filled with water rather than air (Knight *et al.*, 1997). Thus the dry soil conditions at time of installation for the buriable TDR sensors may have resulted in poor installation of the buriable TDR sensors, resulting in air gaps which introduce further errors in the measurements, especially under wet soil conditions.

A comparison of soil moisture measurements made with the Virrib sensors has also been made by Brian Loveys of CSIRO Horticulture. The sensors used for this comparison were the Theta Probe and CS615 reflectometer. The results of this comparison are given in Figure 9.25, indicating that the Virrib measurements

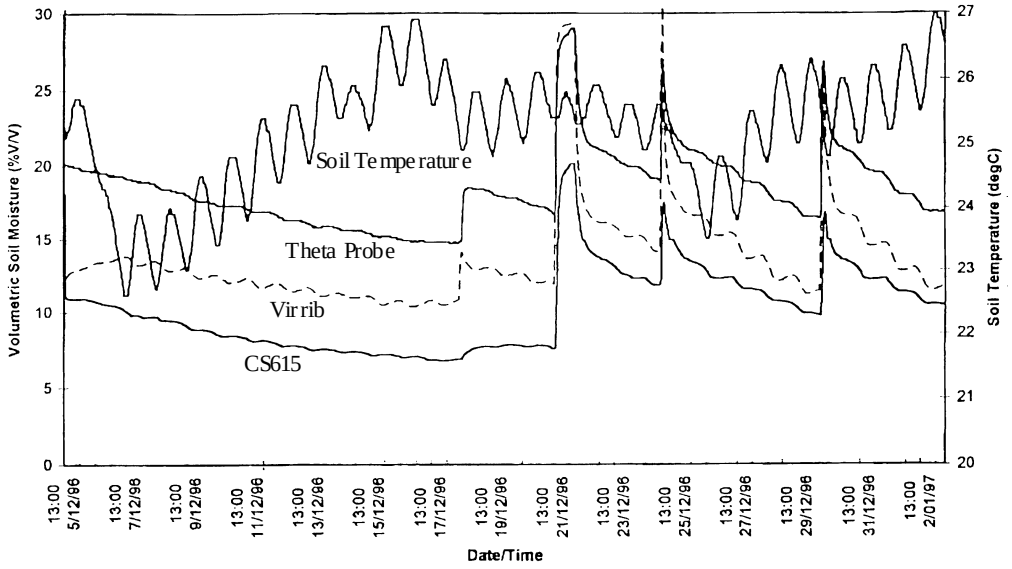

Figure 9.25: Comparison of Theta Probe, Virrib and CS615 reflectometer (Brian Loveys, Personal communication).

were consistently wetter than the CS615 reflectometer measurements by between 2 to 5% v/v and that the Theta probe measurements were consistently wetter then the Virrib measurements by approximately 5% v/v, except for periods of infiltration.

9.3.2 SPATIAL DISTRIBUTION OF SOIL MOISTURE

The spatial distribution of soil moisture content in the Nerrigundah catchment was monitored in three ways:

i) The TRASE TDR system with 15 cm connector TDR probes was used to monitor the spatial distribution and temporal variation of near-surface soil moisture content within the Nerrigundah catchment on a 20 m $\times$ 20 m grid during the intensive soil moisture mapping field campaign. This was achieved using the University of Melbourne's Terrain Data Acquisition System (TDAS), affectionately known as the "Green Machine" (Western *et al.*, 1996a). This system consists of an all terrain vehicle (Figure 9.26) with a position fixing system that allows the operator to drive to pre-determined sample locations.

ii) Connector TDR probes of increasing lengths were installed at 12 locations within the Nerrigundah catchment (in addition to those at the weather

a)

b)

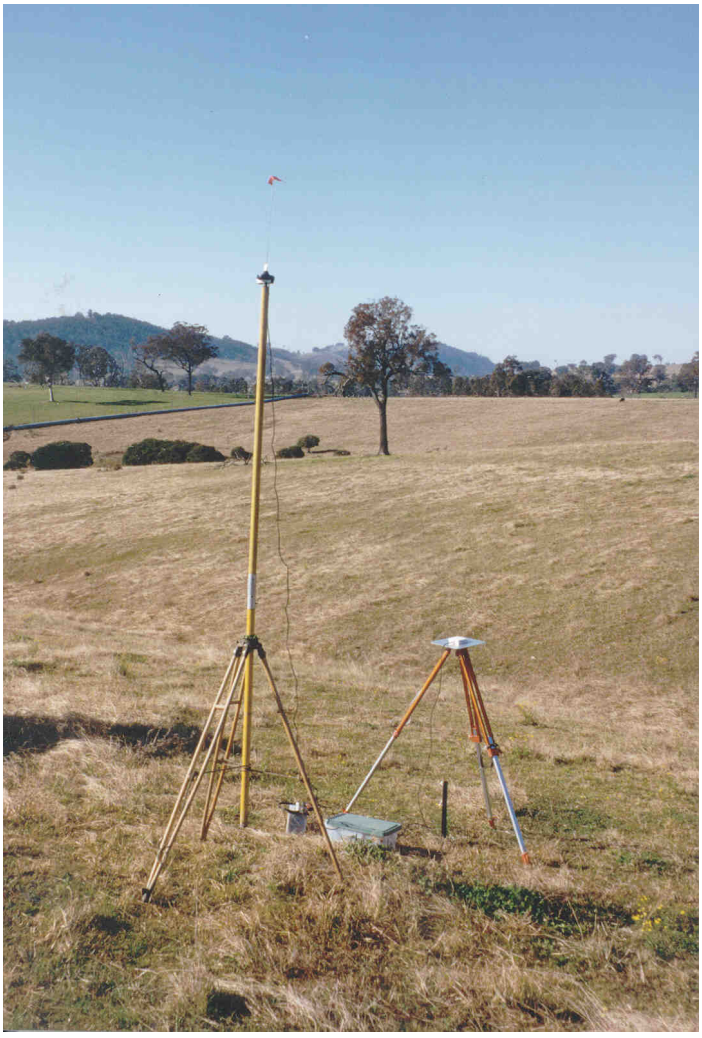

Figure 9.26: Terrain data acquisition system. a) The “Green Machine”; b) GPS base station.

station) for monitoring of soil moisture profiles down to the lesser of depth to bedrock or 1 m depth. Soil depth at these locations was determined from probing with a 6 mm steel rod.

iii) ERS-2 data was obtained for all overpasses during the intensive soil moisture mapping campaign.

9.3.2.1 Green Machine Data

Average soil moisture content over the top 15 cm of the soil profile was measured using connector TDR probes on a 20 m × 20 m sampling grid from August 27 1997 to September 22 1997. Soil moisture mapping was undertaken on Julian days 239 (August 27), 241, 244, 246, 249, 251, 253, 255, 258, 260, 262 and 265, with the mapping taking 6 to 8 hours. Plots of the soil moisture mapping, interpolated soil moisture maps, and differences in soil moisture between soil moisture mappings are given in Appendix C. An example of the soil moisture maps produced is given in Figure 9.27. This data is used for updating of the soil moisture profile forecasts (Chapter 11) from the simplified soil moisture profile model developed in Chapter 7, using the Modified Kalman-filter developed in Chapter 8.

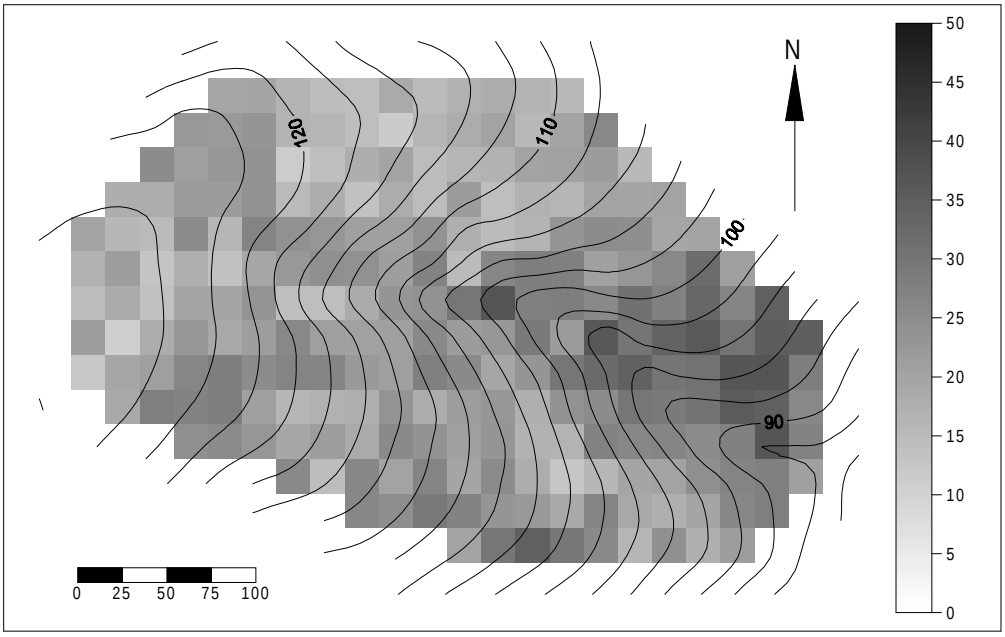

Figure 9.27: Soil moisture map of Nerrigundah catchment on Julian day 258 1997.

Meteorological data collected during the intensive field campaign is given in Figure B.9, for interpretation of the soil moisture maps. This data is also given for later reference when discussing modelling results from the intensive field campaign (Chapter 11). The meteorological data shows that while there was a small amount of rain during the first 22 days of the 25 day intensive field campaign, there was a general drying out of the soil moisture profile. During the last 3 days of the intensive field campaign, approximately 20 mm of rainfall was observed, causing a general wetting up of the near-surface soil layer.

The rainfall during the first 22 day period fell between soil moisture mappings. Hence, soil moisture measurements made during this period should be representative of a "snap shot" of the spatial variation of near-surface soil moisture content. However, 7.5 mm of rain fell during the soil moisture mapping process on Julian day 262. The effect of this rainfall on the soil moisture mapping data is clearly evident in Figure 9.28, which shows the soil moisture difference between Julian days 260 and 262 (Figure 9.28a) and between Julian days 262 and 265 (Figure 9.28b). Furthermore, the difference plots clearly show the effect of the sampling strategy given in Figure 9.29, as a result of rainfall.

The soil moisture maps in Appendix C for the intensive 25 day field campaign show a persistent spatial pattern of catchment wetness, with the north-eastern portion of the catchment and lower reaches of the main drainage line having persistently wetter soil moisture contents. This soil moisture pattern correlates with the spatial variation in soil depth (Figure 9.44). The persistently dry soil moisture measurement in the south-east section of the catchment corresponds with the large tree in Figure 9.4.

The soil moisture maps in Appendix C have not displayed any obvious dependence on aspect, although Western *et al.* (1996b) have noted that this was an influencing factor in the Tarrawarra catchment. Western *et al.* (1997b) have also noted that during wetter periods the soil moisture patterns appear more dominated by topography, while in drier periods the patterns appear much more random, with the transition between the wet and dry state occurring rather quickly. This was also observed for Nerrigundah, with the catchment going from dry to wet in about 3 days.

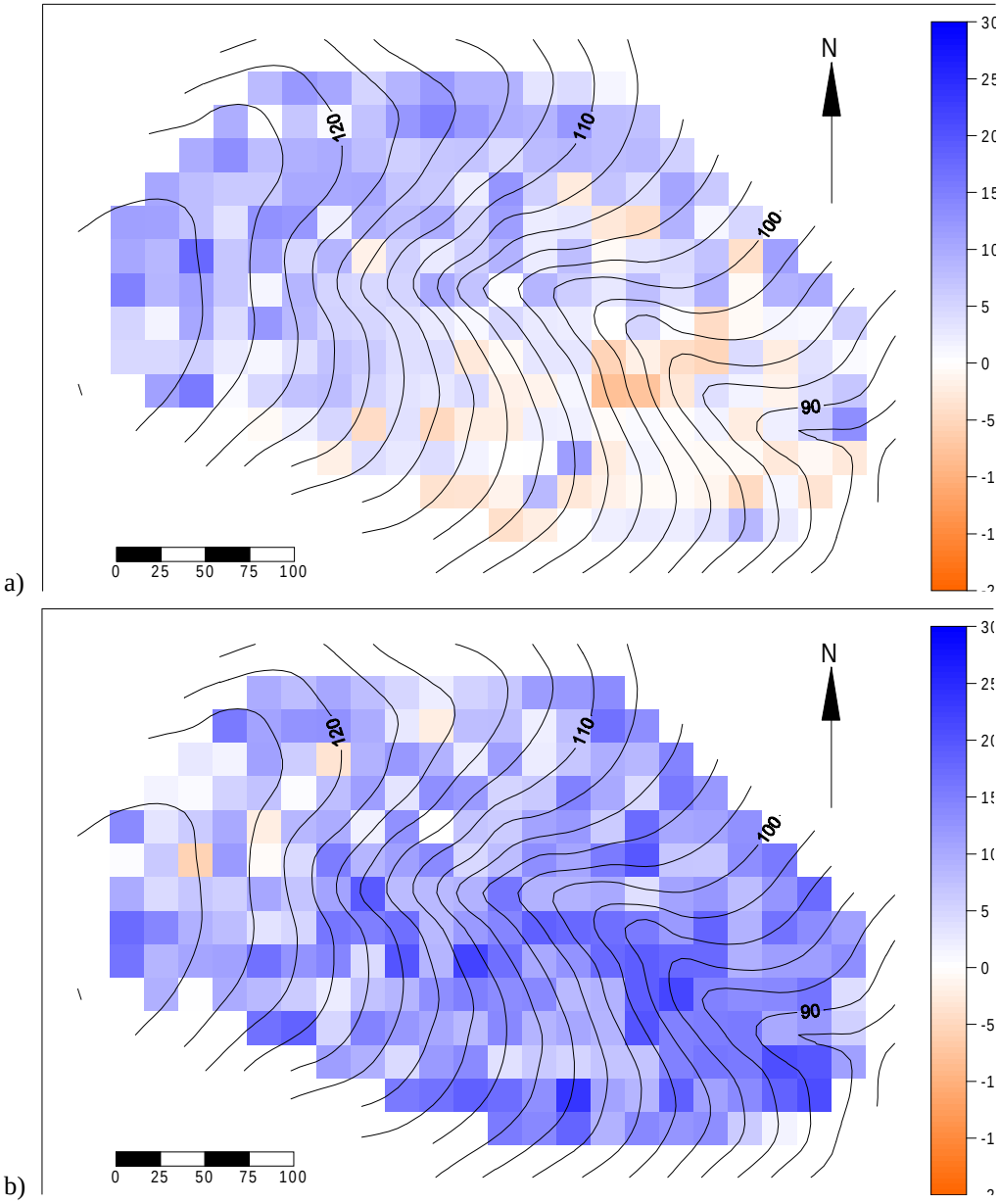

Figure 9.28: Soil moisture difference plots: a) Julian day 260 to 262; b) Julian day 262 to 265.

These observations in the Tarrawarra catchment, along with analysis of data from other locations, have formed the basis of a hypothesis that soil moisture patterns in temperate regions switch between two preferred states (Grayson *et al.*, 1997). The wet state is dominated by lateral movement of water through both surface and sub-surface paths, with catchment terrain leading to organisation of wet areas along drainage lines (see Figure C.12). The dry state is dominated by vertical fluxes, with soil properties and only local terrain influencing the spatial patterns. This dry state occurs in the periods when evapotranspiration continually exceeds precipitation, with the soil moisture patterns reflecting soil and vegetation

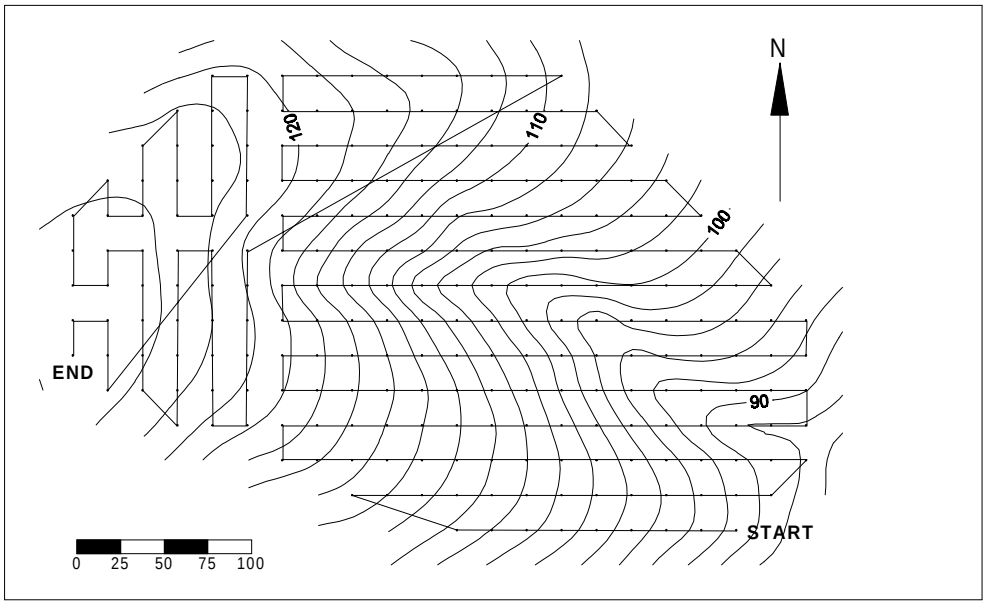

Figure 9.29: Soil moisture sampling strategy.

differences, taking on a more random appearance (see Figure C.2). As evapotranspiration decreases and/or rainfall increases, the areas of high local convergence are the first to become wet. These areas are generally in the upper reaches of the catchment near the ends of depression lines. As these areas become wet, a progressively smaller amount of rain is needed to generate runoff. At some point, runoff is generated and moves down the depression, rapidly saturating the drainage lines from above (Grayson *et al.*, 1997). This hypothesis is consistent with data collected in the Nerrigundah catchment.

In modelling soil moisture content, it is necessary to have some idea of both the sub-grid and inter-grid variability in the system being modelled. For a grid resolution of 20 m, sub-grid variability is the variability in soil moisture content over distances less than 10 m, whilst inter-grid variability is the variability in soil moisture content over distances greater than 20 m.

To investigate the sub-grid variability, the differences in soil moisture measurements for 25 m transects with measurements every 0.5 m (Figure 9.22 and Figure 9.23), and 5 m transects with measurements every 0.1 m (Figure 9.24), have been assessed. Inter-grid variability was estimated by assessing the differences between grid point measurements of soil moisture content from the soil moisture mappings on a given day.

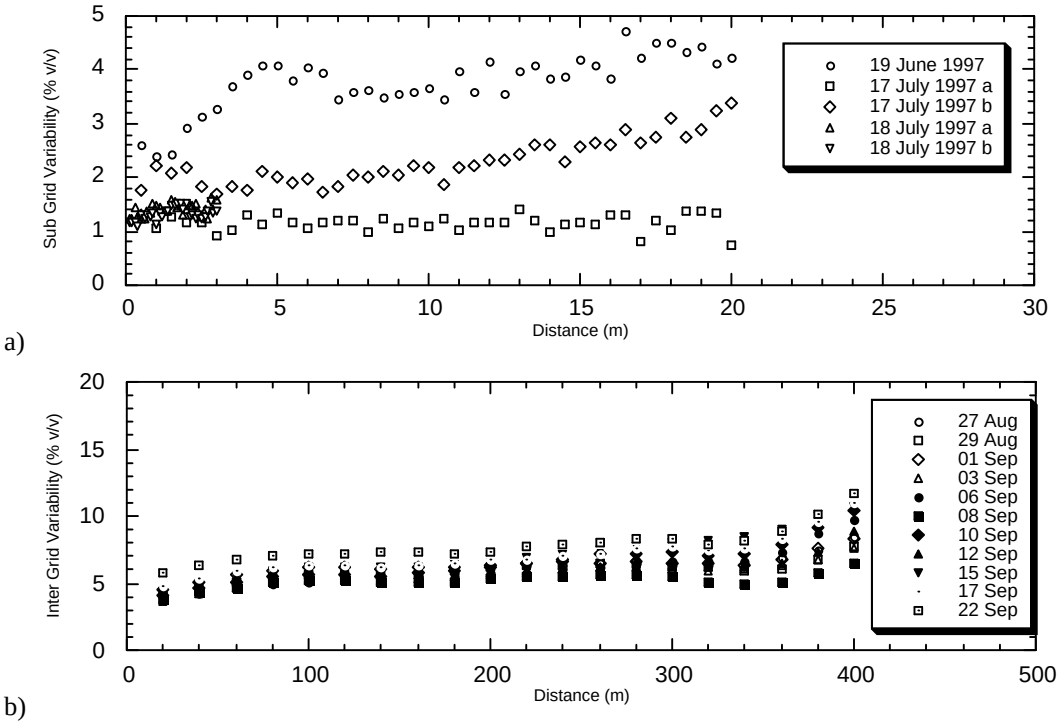

Figure 9.30: a) Sub-grid variability; b) Inter-grid variability.

The average difference in soil moisture content at increasing distances is given in Figure 9.30a for sub-grid variability and Figure 9.30b for inter-grid variability. These results show that apart from the saturated conditions on June 19, the sub-grid variability was approximately 1 to 2% v/v with a standard deviation of ±1 to 2% v/v. This variability was also constant within the ±10 m, but started to increase for greater distances. Hence the sub-grid variability was approximately that of the measuring device. The inter-grid variability indicated in Figure 9.30b began at approximately 5% v/v and increased to approximately 10% v/v at a distance of 400 m, with a standard deviation of 5% v/v. This inter-grid variability was more than double that of the sub-grid variability, which would suggest that a grid resolution of 20 m was appropriate for the Nerrigundah catchment.

9.3.2.2 Profile Soil Moisture Data

The spatial variation of soil moisture profiles was monitored with permanently installed TDR probe lengths of 5, 10, 15, 20, 30, 40, 50, 60, 70, 80 and 100 cm. Soil moisture profiles were measured on Julian days 234 (August 22 1997), 239, 241, 244, 246, 249, 251, 253, 255, 258, 260, 262, 265, 267, 287, 301, 330, 357, 35, 77, 91, 118, 127, 141, 170, 203 and 293 (October 20 1998). These

profile measurements of soil moisture content monitoring began before the TDAS monitoring of near-surface soil moisture content commenced (Julian day 241), in order to give a background estimate of the spatial variation of soil moisture profiles. During the field campaign, soil moisture profile measurements coincided with near-surface soil moisture measurements, for evaluation of the spatially distributed soil moisture profile estimation algorithm at updating times. Monitoring of soil moisture profiles was continued after the intensive field campaign for calibration of the hydrologic model, to data independent of that for which the evaluation was applied. The locations of soil moisture profile measurement sites can be seen in Figure 9.4, with AMG coordinates and soil depth given in Table B.2. Soil moisture profile monitoring sites were located in these positions, which are primarily along fence lines, so they would not get disturbed.

Figure B.10 contains plots of the soil moisture profile measurements for the various probe lengths at all soil moisture profile monitoring sites. No calibration was applied to the measurements. The plots show a wide range of variation in soil moisture content across the catchment, with TDR probe lengths of 5 cm having the greatest variation, being approximately 20% v/v. This is to be expected given the calibration results for the 5 cm probe. Other probe lengths have a variation of approximately 15% v/v.

9.3.2.3 ERS-2 Data

The ERS-2 overpasses, which occurred within the intensive field monitoring of the spatial distribution of soil moisture content, were on Julian days 249 at 12:59 and 265 at 12:56 (Australian eastern standard time). These overpasses coincided with two of the ground based near-surface soil moisture mapping missions. Quick-look images of this data are given in Figure B.11 and Figure B.12.

Although the SAR signal is influenced by only the top few centimetres of soil moisture content and TDR measurements were made over the top 15 cm, providing the soil moisture is relatively wet or relatively dry, the 15 cm measurements are indicative of the soil moisture content in the top few centimetres (Western *et al.*, 1997b).

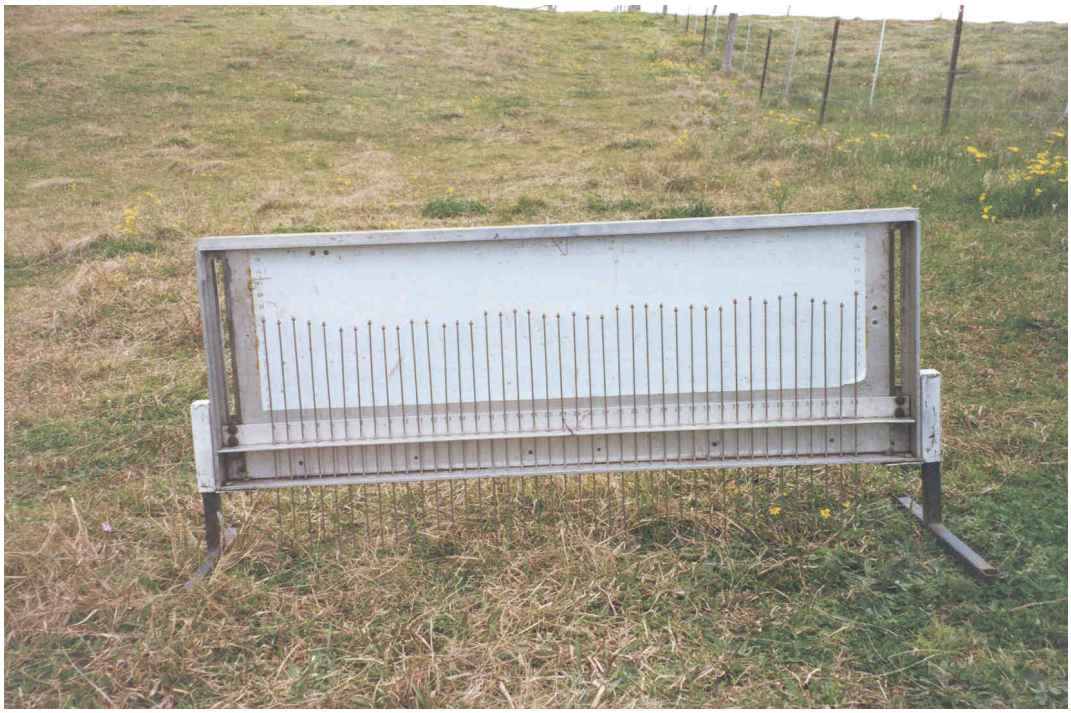

Figure 9.31: Drop pin profiler used for surface roughness measurements.

Surface roughness measurements were made at 5 locations for each of the satellite overpasses using a 1 m long drop pin profiler with a pin separation of 25 mm. The drop pin profiler used is shown in Figure 9.31. Two sets of 1 m measurements were made in, north south, east west, and north east - south west directions, at each of the 5 locations. The roughness measurements were made near soil moisture profiles 2, 5, 7, 8 and 9 (see Figure 9.4). This data is presented in Appendix D, with an example surface roughness profile given in Figure 9.32. While surface roughness measurements are essential for interpretation of the SAR data, they also provide a measure of the depression storage in the catchment. An estimate of depression storage is necessary for application of the hydrologic model developed in Chapter 7.

A visual inspection of the Nerrigundah catchment indicated that the spatial distribution of surface roughness was uniform, apart from the main drainage line and steeper portions of the site. These portions were slightly rougher as a result of cattle grazing. This increased roughness in the gully is also seen in the roughness measurements made near soil moisture profile number 8. However, there is a wide variation in the roughness measurements, even for consecutive surface roughness profile segments at the same site, for the same direction, and for the same day.

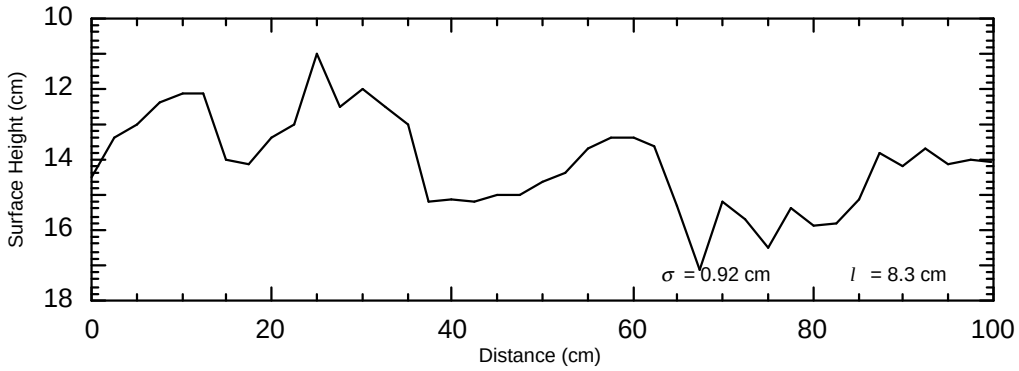

Figure 9.32: Example of roughness data with rms roughness height σ and correlation length l

Whilst two SAR images is an insufficient number for testing of any data assimilation scheme, they may be used for studies on near-surface soil moisture content measurement capabilities with ERS-2 SAR data. In addition, collection of this data has resulted in the compilation of a complete and useful data set, which may be used for many future studies.

Time constraints have not permitted any analysis of the SAR data in this thesis. However, it is envisaged that these two images may be used to evaluate the procedure suggested by Lin (1994) for estimating surface roughness parameters (see section 2.4.5.5). The image collected on Julian day 249 would be used in conjunction with the ground measured soil moisture data to invert for surface roughness parameters. The inverted surface roughness parameters would then be used to compare with ground measured surface roughness, and inversion of backscattering observations on Julian day 265 for near-surface soil moisture content. The inverted soil moisture content would then be compared with the ground measured soil moisture content on Julian day 265. In addition, these images could be used for evaluation of backscattering models, and investigation of the effect of changes in local incidence angle as a result of topography.

9.4 EVAPOTRANSPIRATION

Evapotranspiration refers to evaporation and transpiration lumped together. Two standard evapotranspiration rates are defined, potential evapotranspiration and actual evapotranspiration, and are used as the basis for evapotranspiration estimates. Potential evapotranspiration refers to the amount of

evapotranspiration that would occur as a response to atmospheric demand when there is an unlimited supply of water, while actual evapotranspiration is the amount of evapotranspiration that actually occurs.

Methods for measuring the actual evapotranspiration flux include the Bowen ratio and eddy correlation methods. However, these data are not available from standard meteorological sites. Other methods for estimating actual evapotranspiration, such as the Penman-Monteith combination equation, require calibration with one of the above methods for accurate estimation of parameters such as the crop resistance.

In order to apply the soil moisture estimation algorithm over large areas in an operational setting, it is necessary to apply simple evapotranspiration models that require only standard meteorological data as input, such as that collected by the automatic weather station in the Nerrigundah catchment. Two alternatives for estimating actual evapotranspiration were investigated for applicability. These are the soil moisture stress index and bulk transfer methods.

9.4.1 SOIL MOISTURE STRESS INDEX METHOD

By the soil moisture stress index method, evapotranspiration is assumed to be at its potential level as long as the available water is equal to the maximum available water. Therefore, the potential evapotranspiration rate is reduced to the actual evapotranspiration rate by a relationship with the actual moisture state of the soil (Maidment, 1992).

$$ET_a = SI \times ET_P \qquad (9.1)$$

where ET_a is the actual evapotranspiration, ET_P is the Penman-Monteith potential evapotranspiration, and SI is a soil moisture stress index. Several forms of the soil moisture stress index have been presented in literature. However, this approach has been the subject of criticism over the last 20 years because of the process of cause and effect, as the actual evapotranspiration rate affects the climatic factors used to calculate the potential evapotranspiration (Morton, 1969).

9.4.1.1 Soil Moisture Stress Indices

Common forms of the soil moisture stress index are given below. Ragab (1995) has used

$$SI = \left[\frac{\theta - \theta_{wp}}{\theta_{fc} - \theta_{wp}} \right] \qquad (9.2a),$$

where θ is the volumetric moisture content of the near-surface soil, θ_{wp} is the wilting point soil moisture content and θ_{fc} is the field capacity soil moisture content. Ottlé *et al.* (1989) have used

$$SI = \min\left(1, \frac{3}{2}\frac{\theta}{\phi}\right) \qquad (9.2b),$$

where θ is the volumetric moisture content of the near-surface soil and ϕ is the soil porosity. Another soil stress index is (Kalma *et al.*, 1995)

$$SI = \left(\frac{\theta}{\phi}\right)_{total\ depth} \qquad (9.2c),$$

where θ is the integrated volumetric soil moisture content over the total soil profile depth and ϕ is the average soil porosity over that depth.

9.4.1.2 Penman-Monteith Combination Equation

The Penman-Monteith combination equation for actual evapotranspiration ET_a (cm s^{-1}) is given by (Smith, 1991)

$$ET_a = \frac{\Delta\left(R_{net} - q_h\right) + \rho_{air} c_a \left(e_a - e_d\right)\frac{1}{r_a}}{L\left[\Delta + \gamma\left(1 + r_c / r_a\right)\right]} \qquad (9.3a),$$

where R_{net} is the net radiation flux at the soil surface (cal cm^{-2} s^{-1}), q_h is the soil heat flux (cal cm^{-2} s^{-1}) and c_a is the specific heat capacity of moist air

(0.242 cal g^{-1} °C^{-1}). The saturation partial vapour pressure e_a (kPa) is given by (Smith, 1991)

$$e_a = 0.611 \exp\left(\frac{17.27 T_{air}}{T_{air} + 237.3} \right) \quad (9.3b),$$

where T_{air} is the air temperature (°C). The dew point partial vapour pressure e_d (kPa) is given by (Smith, 1991)

$$e_d = RH_{air} e_a \quad (9.3c),$$

where RH_{air} is the relative humidity of the air. The air density ρ_{air} (g cm^{-3}) is given by (Brutsaert, 1982)

$$\rho_{air} = \frac{P_{atm}}{100 R_d (T_{air} + 273)} \left(1 - \frac{0.378 e_d}{P_{atm}} \right) \quad (9.3d),$$

where P_{atm} is the atmospheric pressure (kPa), R_d is the specific gas constant of dry air (2.8704×10^6 erg g^{-1} °C^{-1}). The latent heat of vaporisation L (cal g^{-1}) is given by (Milly, 1982)

$$L = L_{ref} - (c_l - c_p)(T_{air} - T_{ref}) \quad (9.3e),$$

where L_{ref} is the latent heat of vaporisation (cal g^{-1}) at a reference temperature T_{ref} (°C), which can be taken as 591.6 cal g^{-1} at 10°C (Monteith and Unsworth, 1990). c_p is the specific heat of water vapour (0.449 cal g^{-1} °C^{-1}) and c_l is the specific heat capacity of liquid water (1.0 cal g^{-1} °C^{-1}; Monteith and Unsworth, 1990). The slope of the vapour pressure curve Δ (kPa °C^{-1}) is given by (Smith, 1991)

$$\Delta = \frac{4098 e_a}{(T_{air} + 237.3)^2} \quad (9.3f).$$

γ is the psychometric constant (kPa °C^{-1}) given by (Smith, 1991)

$$\gamma = \frac{c_p P_{atm}}{\in L} \times 10^{-3} \qquad (9.3g),$$

where $\in$ is the ratio of molecular weight of water vapour to dry air (0.622). The aerodynamic resistance r_a (s cm^{-1}) is given by (Smith, 1991)

$$r_a = \frac{\ln\left(\frac{z_U - d_o}{z_{om}}\right)\ln\left(\frac{z_T - d_o}{z_{ov}}\right)}{k^2 U} \qquad (9.3h),$$

where z_U is the height of wind speed measurements (cm), z_T is the height of temperature and humidity measurements (cm), k is the von Karmen constant (0.41) and U is the wind speed measurement (cm s^{-1}). The zero plane displacement of the wind profile d_o (cm) is given by (Smith, 1991)

$$d_o = \frac{2}{3} h_c \qquad (9.3i),$$

where h_c is the crop height (cm). The roughness parameter for momentum z_{om} (cm) is given by (Smith, 1991)

$$z_{om} = 0.123 h_c \qquad (9.3j).$$

The roughness parameter for heat and water vapour z_{ov} (cm) is given by (Smith, 1991)

$$z_{ov} = 0.1 z_{om} \qquad (9.3k).$$

For estimation of the potential evapotranspiration ET_p from the Penman-Monteith combination equation, the crop resistance r_c is taken as zero.

9.4.2 BULK TRANSFER METHOD

Like the soil moisture stress index method, the bulk transfer method also only requires standard meteorological observations. The bulk transfer method for estimation of actual evapotranspiration ET_a (cm s^{-1}) is given by (Brutsaert, 1982)

$$ET_a = \rho_{air} C_E U (q_S - q_T) \quad (9.4a),$$

where ρ_{air} is the air density (g cm^{-3}), C_E is a unitless moisture transfer coefficient, U is the wind speed (cm s^{-1}) at height z_U (cm), q_S is the specific humidity at the soil surface as a function of near-surface soil temperature T_S, and q_T is the specific humidity in the air at height z_T.

The bulk transfer method has generally been applied to evaporation from lakes (Brutsaert, 1982), with the surface specific humidity as the saturated specific humidity for the water surface temperature. However, the surface specific humidity may be estimated by (Braud, 1996)

$$q_S = \frac{0.622 \mathrm{e_S} RH_S}{P_{atm} - 0.378 \mathrm{e_S} RH_S} \quad (9.4b),$$

where P_{atm} (kPa) is the atmospheric pressure and $\mathrm{e_S}$ is the saturated vapour pressure (kPa) at the soil surface given by

$$\mathrm{e_S} = 0.611 \exp\left(\frac{17.27 T_S}{T_S + 237.3} \right) \quad (9.4c).$$

RH_S is the relative humidity at the soil surface given by the Kelvin law as

$$RH_S = \exp\left(\frac{-g\psi_S}{R_V (T_S + 273)} \right) \quad (9.4d),$$

where g is the acceleration due to gravity (981 cm s^{-2}), R_V is the specific gas constant of water vapour (4.615×10^6 erg °C^{-1}) and ψ_s is the soil matric head (cm) at the soil surface. The soil matric head can be estimated from the volumetric soil moisture measurements by the Clapp and Hornberger (1978) relationship

$$\psi = \psi_s \left(\frac{\theta}{\phi} \right)^{-b} \quad (9.4e),$$

where ψ_s is the saturated soil matric head (cm) and b is a soil texture parameter. Both ψ_s and b were estimated from published data for a silt loam soil as –78.6 cm and 5.3 respectively (see Table B.13). The specific humidity in the air is given by

$$q_T = \frac{0.622 e_a RH_{air}}{P_{atm} - 0.378 e_a RH_{air}} \qquad (9.4f),$$

where the saturation partial vapour pressure e_a (kPa) is given by (9.3b). The moisture transfer coefficient C_E is not a constant, and varies as a function of land surface characteristics as given by

$$C_E = \frac{0.41^2}{\ln\left[\frac{z_T - d_o}{z_{ov}}\right]\ln\left[\frac{z_U - d_o}{z_{om}}\right]} \qquad (9.4g),$$

where z_{ov} is the water vapour roughness length (cm) given by (9.3k), z_{om} is the roughness length for momentum (cm) given by (9.3j) and d_o is a zero plane displacement height (cm) given by (9.3i). The roughness lengths and zero plane displacement level can be estimated from crop height.

A complication of the bulk transfer approach is the need for an estimate of the surface soil temperature, in addition to near-surface soil moisture content. However, the relationship between dielectric constant and soil moisture is also dependent on soil temperature (see Chapter 2) and needs to be estimated for measurement of near-surface soil moisture content from remote sensing. Thus, the need for an estimate of soil temperature does not impose a major limitation on the bulk transfer method for estimating the actual evapotranspiration. However, modelling of soil temperature requires an estimate of the soil thermal properties in addition to the soil hydraulic properties (see Chapter 5).

9.4.3 ESTIMATION OF ACTUAL EVAPOTRANSPIRATION

During the intensive field campaign, eddy correlation measurements of actual evapotranspiration were made on Julian days 244, 246, 249, 251, 260 and 261 (Scott Wooldridge, Personal communication).

To determine which of the methods in the previous sections gives the best estimate of actual evapotranspiration, comparisons were made with eddy correlation measurements and water balance calculations using the Virrib soil moisture measurements. Potential evapotranspiration was estimated from the 10 minute data collected by the automatic weather station.

Three different water balance calculations were made for estimating the cumulative evapotranspiration. The first method (WB#1) summed the changes in soil moisture content over the soil profile, ignoring the effects of rainfall. The remaining methods used different approaches for taking the effects of rainfall on the soil moisture measurements into consideration. The second method (WB#2) added any rainfall that was measured during consecutive soil moisture measurements, to the cumulative evapotranspiration that would otherwise be estimated directly from the soil moisture measurements. The third method (WB#3) set the evapotranspiration as zero for periods where rainfall was measured. Based on the soil moisture data presented previously, calculations assumed a wilting point moisture content of 10% v/v, field capacity moisture content of 45% v/v and average soil porosity of 50% v/v.

Figure 9.33 shows a comparison of the Penman-Monteith potential evapotranspiration with the three soil moisture stress indices given by (9.2a) to (9.2c), the water balance calculations and the bulk transfer method. This comparison confirmed that the potential evapotranspiration was greater than the actual evapotranspiration estimates from the water balance calculations. It also

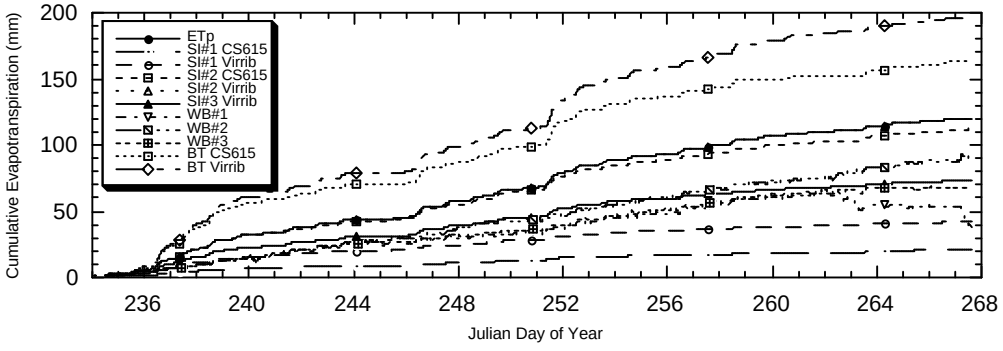

Figure 9.33: Comparison of Penman-Monteith potential evapotranspiration (ETp) with the three different soil stress indices (SI#1 to SI#3), three different water balance approaches (WB#1 to WB#3) and the bulk transfer approach (BT), using both Virrib and CS615 soil moisture data collected during the 1997 intensive field campaign.

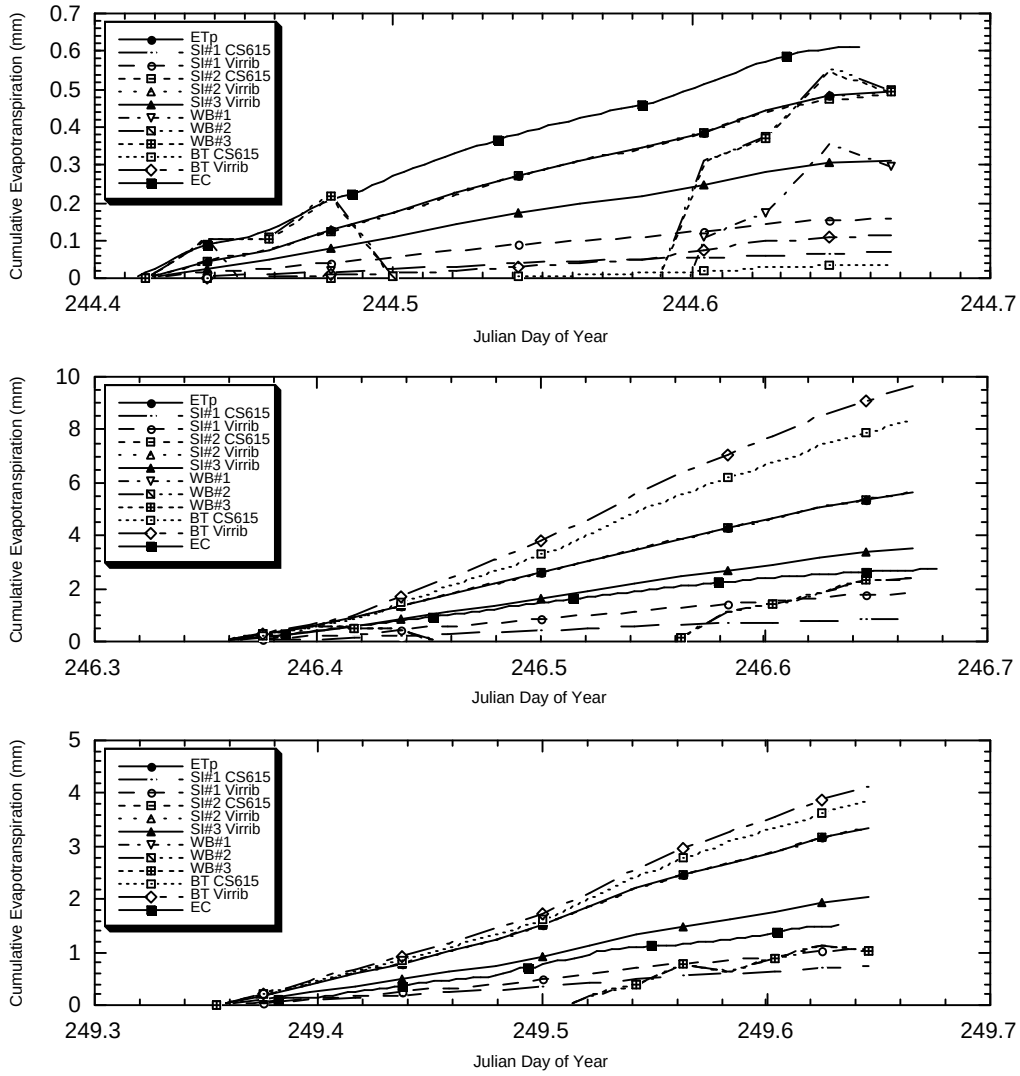

Figure 9.34: Comparison of evapotranspiration estimates in Figure 9.33 with eddy correlation (EC) measurements during the 1997 intensive field campaign.

showed that water balance calculations needed to take account of the rainfall (see WB#1) and that actual evapotranspiration estimates from WB#2 were greater than those from WB#3.

Figure 9.33 also showed that the bulk transfer method over-estimated the actual evapotranspiration, with both bulk transfer estimates being greater than the potential evapotranspiration. As the estimate for actual evapotranspiration should not be greater than the potential evapotranspiration, this would suggest that any assumptions regarding estimation of the relative humidity at the soil surface were of secondary importance. The reason for this is that potential evapotranspiration is defined as evapotranspiration from an unlimited supply of water (ie. RH_s = 1). Hence, an estimate of RH_s less than 1 should result in a reduced estimate of the

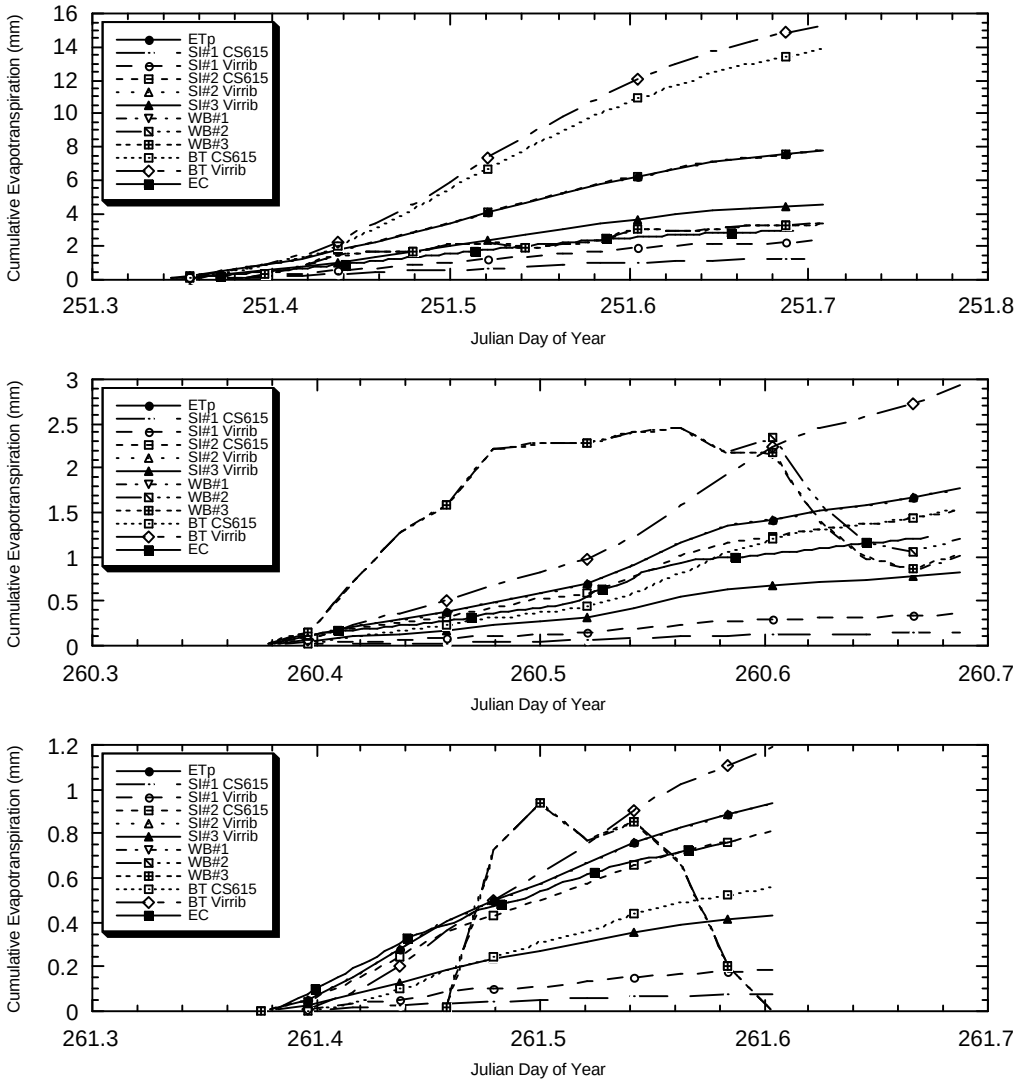

Figure 9.34 (con't): Comparison of evapotranspiration estimates in Figure 9.33 with eddy correlation (EC) measurements during the 1997 intensive field campaign.

actual evapotranspiration. However, other assumptions such as roughness length and wind profile in the moisture transfer coefficient may have made this approach invalid.

It may also be seen from Figure 9.33 that the difference between the potential evapotranspiration and SI#2 was marginal, whilst the actual evapotranspiration estimate from SI#1 was much less than that from the water balance calculations. The actual evapotranspiration estimate from SI#3 however, was between the estimate from WB#2 and WB#3.

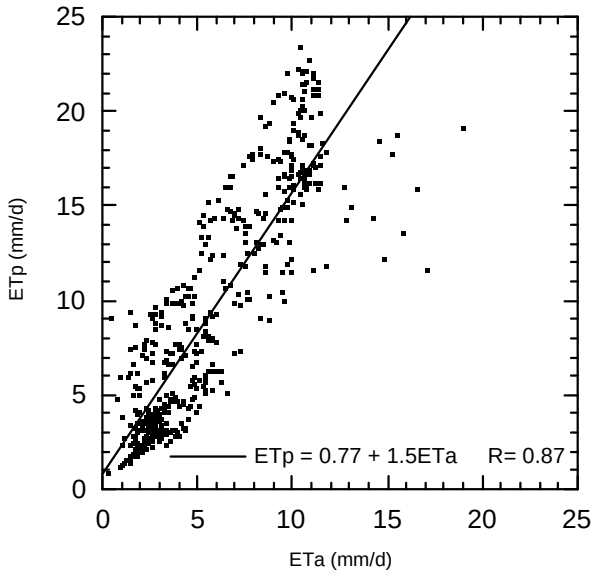

Figure 9.35: Comparison of Penman-Monteith potential evapotranspiration (ETp) with eddy correlation actual evapotranspiration (ETa).

The comparisons with the eddy correlation measurements of actual evapotranspiration in Figure 9.34 revealed several things. Firstly, the water balance calculations displayed diurnal fluctuations in evapotranspiration on most days as a result of diurnal fluctuations in soil moisture profile measurements. Secondly, the eddy correlation measurement of actual evapotranspiration was greater than the potential evapotranspiration on Julian day 244. Most confidence is placed in the eddy correlation measurements on Julian days 246 and 251, as these were cloud free days. On these days, there was a good agreement with SI#3 and the water balance estimates of actual evapotranspiration. Diurnal effects on the water balance calculations were less noticeable on these days due to an increase in the total evapotranspiration during the observing period.

To confirm that the relationship between actual and potential evapotranspiration was linear, Penman-Monteith potential evapotranspiration was plotted against the eddy correlation measurements of actual evapotranspiration for all days of observation (Figure 9.35). Whilst the plot shows some scatter, the assumption of a linear relationship between potential and actual evapotranspiration is defensible.

In summary, Figure 9.34 displayed that SI#3 gave the best estimate of actual evapotranspiration during the intensive field campaign, and Figure 9.35

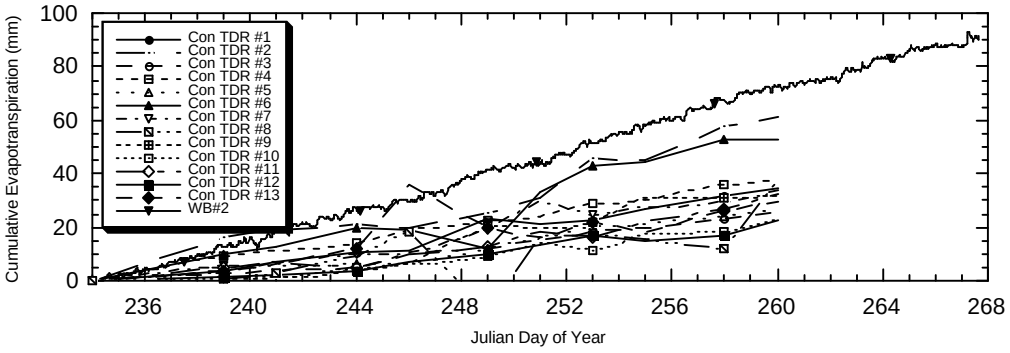

Figure 9.36: Comparison of actual evapotranspiration estimates across the Nerrigundah catchment during the 1997 intensive field campaign using the second water balance approach with the 13 connector TDR (Con TDR) and the Virrib (WB#2) soil moisture measurements.

confirmed that it was appropriate to use a linear stress index relationship. Hence, SI#3 (9.2c) was used for estimation of actual evapotranspiration in the field applications presented in Chapter 10 and Chapter 11.

To investigate the spatial variation of actual evapotranspiration across the Nerrigundah catchment, the second water balance approach using the Virrib soil moisture measurements (WB#2) was applied to the 13 connector TDR measurements made throughout the catchment (see Figure 9.4). The results in Figure 9.36 revealed that actual evapotranspiration estimates from the connector TDR probes were less than those from the Virrib sensors (ie. Con TDR #2), and that there was a wide variation in actual evapotranspiration across the catchment.

9.5 SOIL HEAT FLUX

An estimate of soil heat flux at the soil surface was required for estimating the potential evapotranspiration. Soil heat flux can be determined by several methods, as described by Kimball and Jackson (1979). The methods used were: (i) calorimetric method; (ii) heat flux plate method; (iii) combination method; and (iv) null-alignment method.

9.5.1 CALORIMETRIC METHOD

Using the calorimetric method, the average soil heat flux over a given time interval is computed from the change in heat content of the soil profile during the interval. The profile is divided into layers (Figure 9.37), and the change in

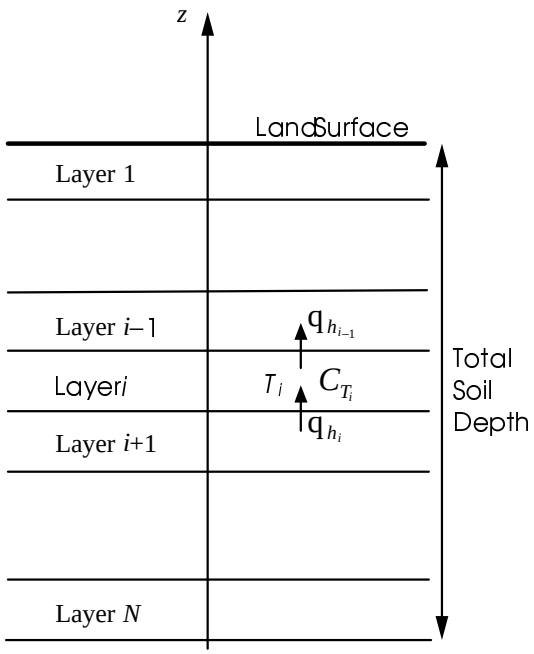

Figure 9.37: Discretisation for estimation of soil heat flux.

temperature of each layer is measured over the interval. The heat flux leaving the top of a soil layer $q_{h_{i-1}}$ (positive upward) is equal to the heat flux entering the bottom q_{h_i} plus the change in heat content per unit time.

$$q_{h_{i-1}} = q_{h_i} + C_{T_i}(z_i - z_{i-1})\left(\frac{T_i^{n+1} - T_i^{n}}{t^{n+1} - t^{n}}\right) \qquad (9.5a),$$

where z_i is the depth (cm) to the top of layer i, z_{i-1} is the depth to the bottom of layer i, T_i^{n+1} is the soil temperature (°C) of layer i at time t^{n+1} (s) and T_i^n is the soil temperature of layer i at time t^n. C_{T_i} is the volumetric heat capacity (cal cm^{-3} $°C^{-1}$) of layer i, and may be estimated from the sum of the heat capacities of the individual soil constituents as

$$C_{T_i} = 0.46\theta_{m_i} + 0.60\theta_{o_i} + \theta_i \qquad (9.5b),$$

where θ_{m_i}, θ_{o_i} and θ_i are the volume fraction of soil minerals, organic matter and water respectively for layer i (see Table 9.2).

Using this method, the soil heat flux at any depth in the soil profile may be computed if the soil heat flux at any one depth is known. This reference depth is generally taken to be about 100 cm, where the soil heat flux is considered to be negligible. A major difficulty of the calorimetric method arises when it is used to compute soil heat flux over shorter time periods (15 to 60 min), as the temperature change of the soil at depths greater than 20 cm is too small to be measured accurately (Kimball and Jackson, 1979).

9.5.2 HEAT FLUX PLATE METHOD

Soil heat flux can be measured using a thin plate with a thermopile wound around it, known as a heat flux plate. The soil heat flux is proportional to the temperature difference between the two plate surfaces. A problem with the heat flux plate is that they interfere with the pattern of heat flow in the soil, and the water movement in both liquid and vapour phases. Therefore they cannot be used accurately close to the soil surface (Kimball and Jackson, 1979).

9.5.3 COMBINATION METHOD

With the combination method, heat flux plates are placed in the soil at 5 to 10 cm depth, and the calorimetric method is used to calculate the soil heat flux above (or below) the placement depth. This method is strongly recommended over either the heat flux plate or calorimetric methods used alone. The combination method removes errors associated with the calorimetric method due to inaccurate temperature measurements at deeper depths, and minimises errors associated with the heat flux plate method due to interference of heat and water flow (Kimball and Jackson, 1979).

9.5.4 NULL-ALIGNMENT METHOD

The null-alignment method was developed by Kimball and Jackson (1975) and is based on measurements of soil temperature, volumetric soil moisture content, soil porosity and organic content, in the upper 20 cm of soil. This method dispenses with heat flux plates, which can interfere with water and heat flow even at 5 cm depth (Kimball and Jackson, 1975). This method is based on the relationship

$$q_h = -\lambda \nabla T \qquad (9.6),$$

where λ is the thermal conductivity (cal cm^{-1} s^{-1} $°C^{-1}$) and ∇T is the temperature gradient (°C cm^{-1}).

In the null-alignment method, null points in the soil temperature gradient are used to provide known zero soil heat fluxes at known depths in the soil profile, and the calorimetric method used to calculate the soil heat flux in the remainder of the soil profile. As long as heat movement due to water or water vapour movement is negligible, the soil heat flux can be taken as zero at the null points (Kimball and Jackson, 1975).

To calculate soil heat flux using the null-alignment method, an initial estimate of thermal conductivity at 20 cm depth is used to calculate the 20 cm depth soil heat flux from the temperature gradient at 20 cm using (9.6). The calorimetric method is then used to calculate the soil heat flux for all layers above 20 cm. Soil temperature profiles for those times of day when a zero soil temperature gradient exists somewhere in the top 20 cm are then used to force a null-alignment of zero soil heat flux with the zero soil temperature gradient. Kimball and Jackson (1975) suggest that soil temperature measurements be made at a minimum of 1 cm intervals above 10 cm and 4 cm intervals below 10 cm, but preferably at half of this. This method is reported to be as good as the combination method (Kimball and Jackson, 1979) with results comparing well with direct heat flux measurements at 5 cm, except at noon when the heat flux plates had somewhat larger values (Kimball and Jackson, 1975).

9.5.5 ESTIMATION OF SOIL HEAT FLUX

Soil heat flux was estimated at the top and bottom of the soil column, monitored at the weather station, using both the null-alignment and combination methods. In addition, the soil heat flux was estimated by the null-alignment method for comparison with the soil heat flux plate measurements at 2 and 12 cm. Soil heat flux was also estimated by the combination method using the soil heat flux plate measurements at 12 cm depth, for comparison with the soil heat flux plate measurements at 2 cm depth. This comparison was performed for data collected during the intensive field campaign period in 1997.

As soil temperature sensors were installed at depths of 2 cm and 12 cm, soil heat fluxes could not be estimated at these depths without either ignoring these measurements or using them for interpolating the soil temperature at other depths. Hence, comparisons of soil heat flux for the null-alignment method were made with layer interfaces either side of the required depth.

The comparisons between soil heat flux plate measurements and the null-alignment method in Figure 9.38 show a poor agreement, with the null-alignment estimate of soil heat flux over-estimating the soil heat flux in comparison to soil heat flux plate measurements. The best agreement is made with soil heat flux plate measurements for null-alignment estimates at 5 cm and 14 cm depth, for heat flux plate measurements of 2 cm and 12 cm depth respectively.

The comparisons between soil heat flux plate measurements and the combination method (Figure 9.39) are better than comparisons for the null-alignment method. However, once again the best agreement between the soil heat flux plate at 2 cm was obtained for an estimate at 5 cm.

Figure 9.40 shows a comparison between both the null-alignment and combination method estimates of soil heat flux at both the soil surface and base of the soil column. The comparison at the soil surface appears to be very good while that at the base of the soil profile appears quite poor. However, this is shown (Figure B.13a) to be a result of the plot scale, with the difference between soil heat flux estimates being the same at both the soil surface and base of the soil profile, as expected. Figure B.13b shows that this difference in soil heat flux is different to the difference in soil heat flux between measured and estimated soil heat flux at a depth of 2 cm using the combination method.

This suggests that differences between the null-alignment method, combination method and measured soil heat flux are not a result of incorrect placement depth, but a result of differences in techniques and disturbance to heat and moisture flow as a result of the top plate being too close to the soil surface. In addition, differences between the null-alignment and combination methods may

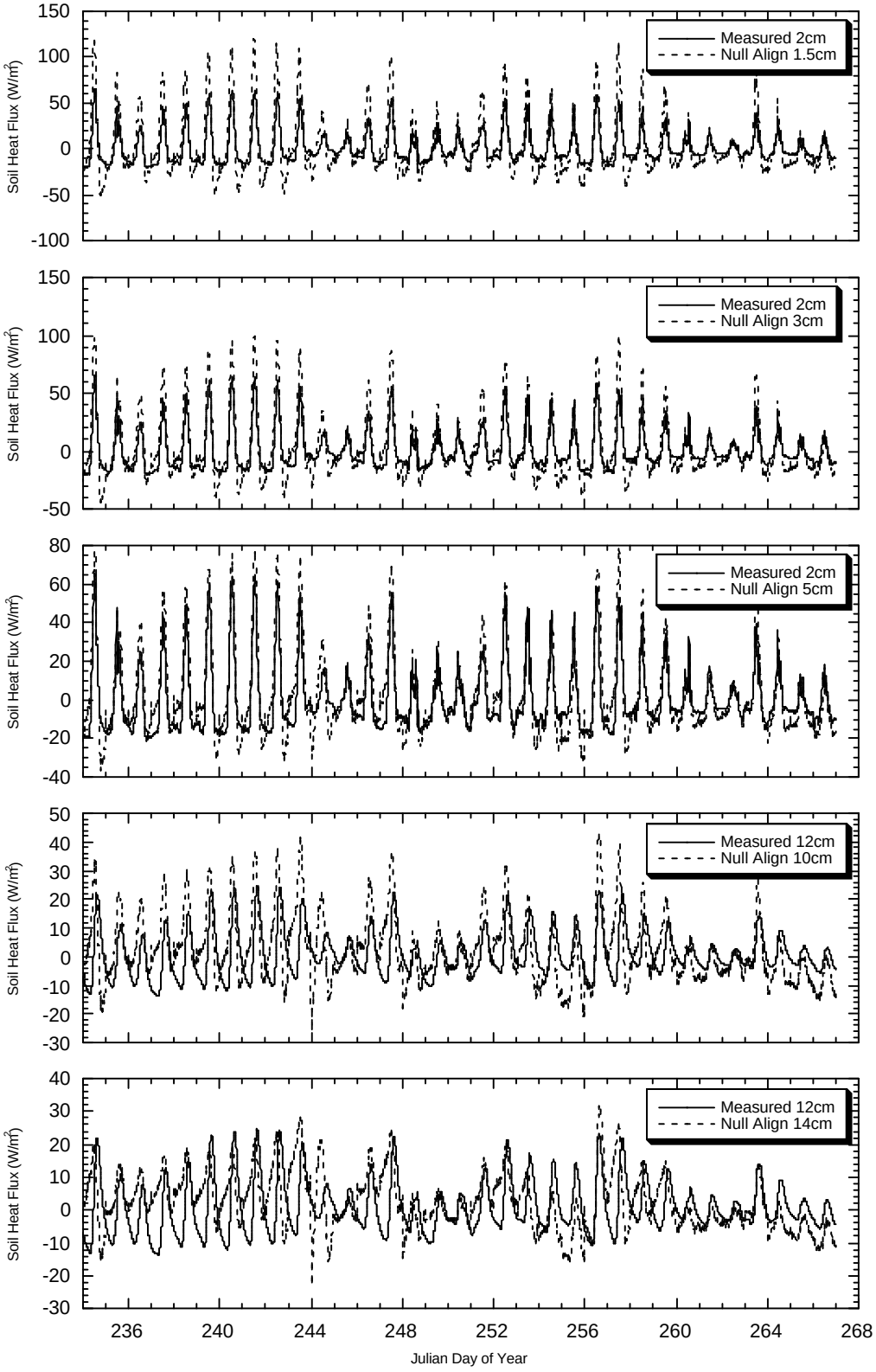

Figure 9.38: Comparison of soil heat flux plate measurements at 2 and 12 cm depth with null-alignment method estimates.

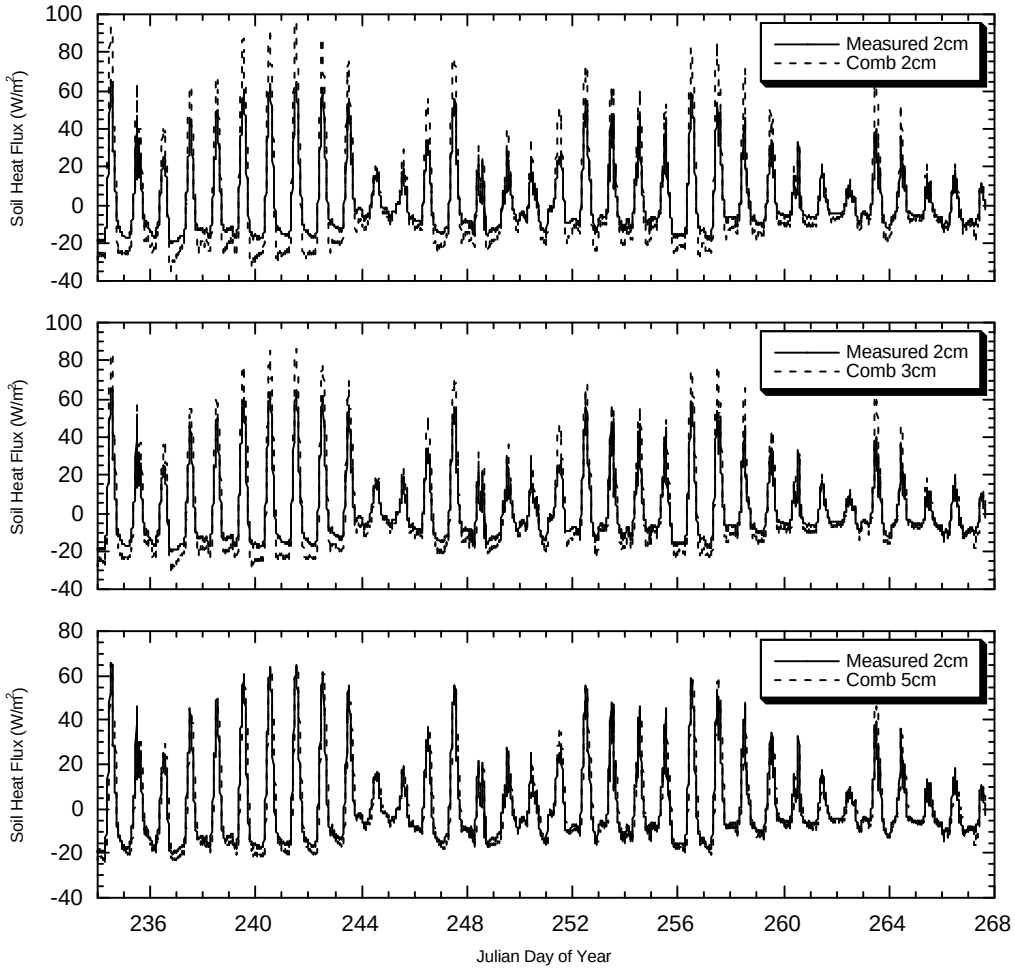

Figure 9.39: Comparison of soil heat flux plate measurements at 2 cm depth with combination method estimates.

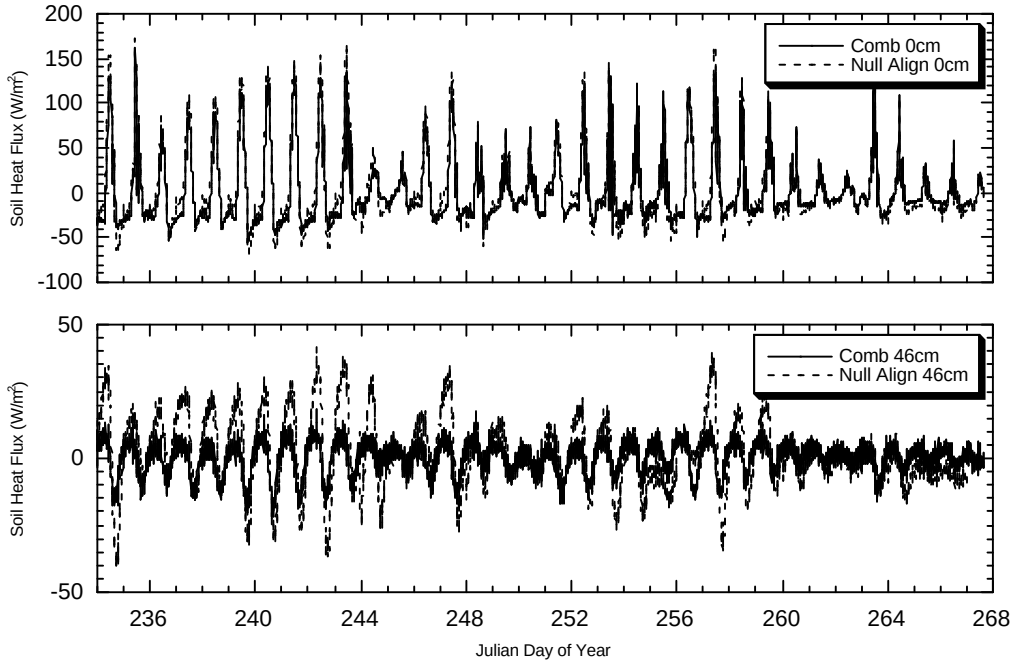

Figure 9.40: Comparison of combination and null alignment method estimates of soil heat flux at the soil surface and soil base.

be a result of the spacing of soil temperature sensors being too large. Hence, soil heat flux has been determined from the combination method for other periods.

9.6 SOIL CHARACTERISATION

Soil characterisation of the Nerrigundah catchment was undertaken from 19 soil cores (see Figure 9.4) retrieved from throughout the catchment using the soil coring capabilities of the TDAS (Western *et al.*, 1996a). The soil coring device of the TDAS is capable of taking a minimally disturbed soil core of 55 mm in diameter and 800 mm in length. The soil corer consists of a rigid steel tube with one end tapered such that the sharpened cutting edge cuts a soil core slightly smaller than the inside diameter of the tube, thus minimising friction and smearing of the soil sample by the tube wall. The tube also has a slight bulge near the base of the taper that compacts the soil around the tube, thereby reducing the insertion force by minimising the friction against the outside of the tube. An illustration of the soil corer is given Figure 9.41 and photographs of the TDAS in soil coring mode are given in Figure 9.42.

As the majority of soil within the Nerrigundah catchment has a depth of less than 600 mm, these soil cores give a view of the entire soil profile at their individual locations. These soil cores were photographed, and overlain onto a contour plan of the catchment (Figure 9.43), for visual assessment and cross-referencing with the laboratory analysis of soil samples.

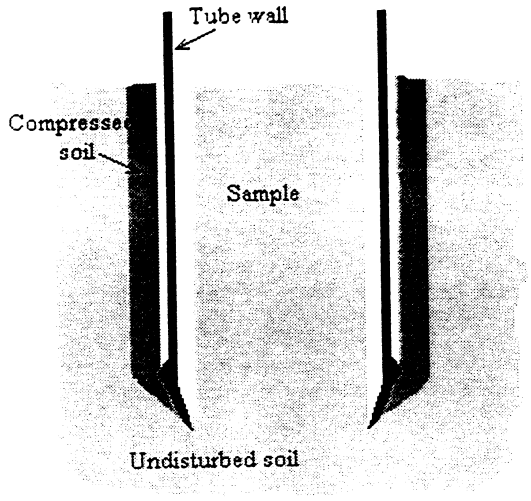

Figure 9.41: Soil corer used by the TDAS (Western *et al.*, 1996a).

a) 

b) 

Figure 9.42: The “Green Machine” in a) soil core retrieval and b) soil core extraction modes.

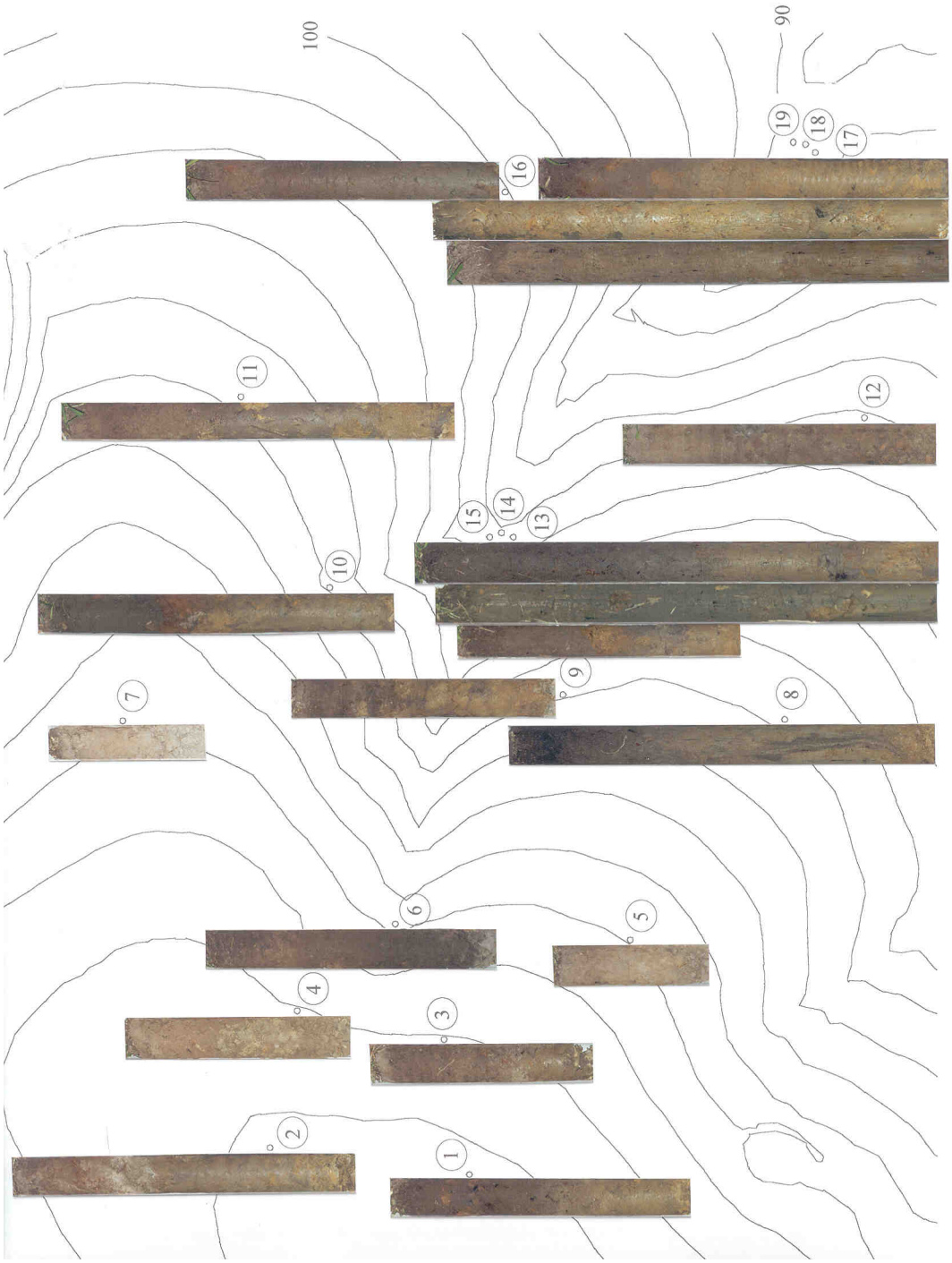

Figure 9.43: Contour plan of the Nerrigundah catchment showing photographs of soil profiles at their location in the catchment.

9.6.1 SOIL DEPTH

The depth of a soil profile varies considerably from one location to another. Soil depth is influenced by many factors, such as parent material, topography, rate of soil formation and soil erosion. Generally, soils at the bottom of a hillslope are deeper than soils at the top and soils formed from hard, resistant parent material will be shallower than those formed from rocks that break down easily.

Total soil depth was determined by measuring the soil cores retrieved using the TDAS. Where the soil depth exceeded 800 mm, further probing was undertaken to estimate the total soil depth. The AMG coordinates for soil core locations and the total soil depth at those locations are given in Table B.3. Soil depth was also estimated from probing with a 6 mm steel rod at profile soil moisture measurement sites, with depths and locations given previously in Table B.2.

Additional soil depths were determined from probing on a 40 m $\times$ 40 m grid (Craig Wood and Michael Kendall, Personal communication) during a period when the soil was moist. These measurements are given in Table B.4. The grid used was coincident with that used for near-surface soil moisture measurement with the TDAS during the intensive field campaign, and soil moisture profile estimation in Chapter 11. Additional measurements were made on a 20 m $\times$ 20 m grid for the area in the vicinity of the main drainage line.

The spatial variation of total soil depth was determined by interpolating onto a 20 m $\times$ 20 m grid, using the soil depth estimates obtained from the soil cores and the soil depth estimates from probing. A plot of total soil depth variation over the Nerrigundah catchment from these point measurements is given in Figure 9.44.

9.6.2 SOIL HORIZONS

After determining total soil depth from the soil cores, the soil profile was described according to its horizons by the Northcote Factual Key Soil Classification System (Northcote, 1979). The organic horizon (O) originates from

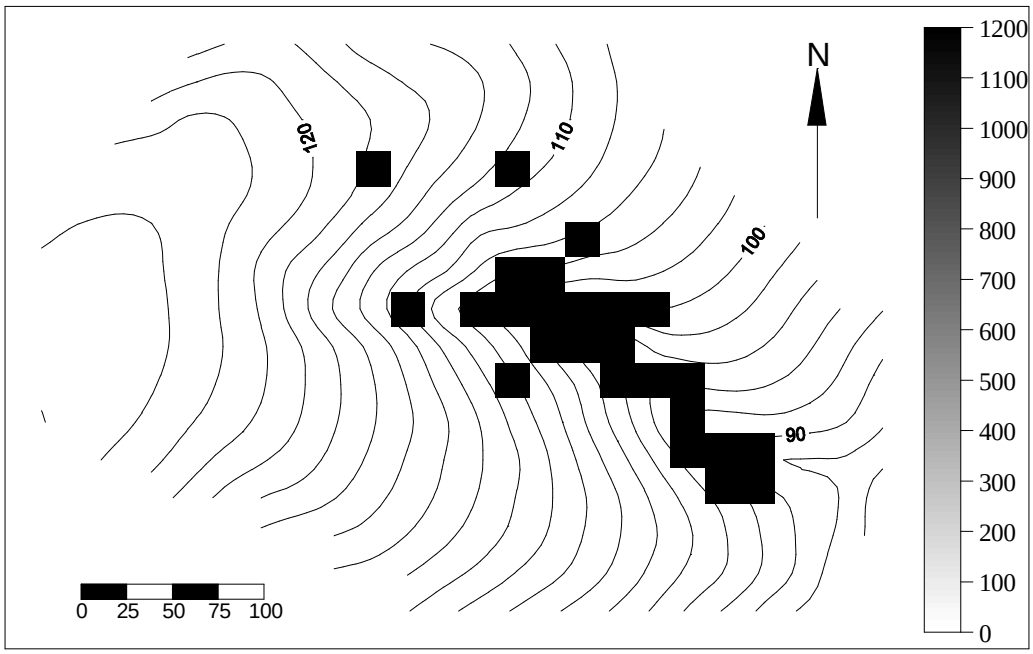

Figure 9.44: Spatial variation of total soil depth (mm) over the Nerrigundah catchment.

dead and decaying organic matter that falls onto the surface from nearby plants. As the study site consisted of open grazing land, the organic horizon was for practical purposes non-existent. The surface horizon (A) is a master horizon consisting of maximum organic accumulation. As a result, this horizon tends to have a dark colour, especially when wet. The A horizon is usually referred to as topsoil and may be divided into a number of sub-horizons, principally A1 and A2. The sub-surface horizon (B) is a horizon of altered and distinct material characterised by more or less block-like or prism-like appearance and structure, together with other characteristics such as strong colours, increased clay content, and poorer drainage. This horizon is known as the subsoil and may be divided into the B1 and B2 horizons. The B1 horizon is a transitional horizon from A to B while the B2 horizon is the main subsoil horizon. The parent material horizon (C) is a master horizon comprising the parent material from which the A and B horizons have been formed.

Thicknesses of soil horizons were noted where identifiable (Table B.5), and the soil core dissected into its horizons for laboratory assessment. Where the A1 horizon was too shallow to give a large enough soil sample for laboratory testing by itself, the A1 and A2 horizons were combined. The spatial variation of

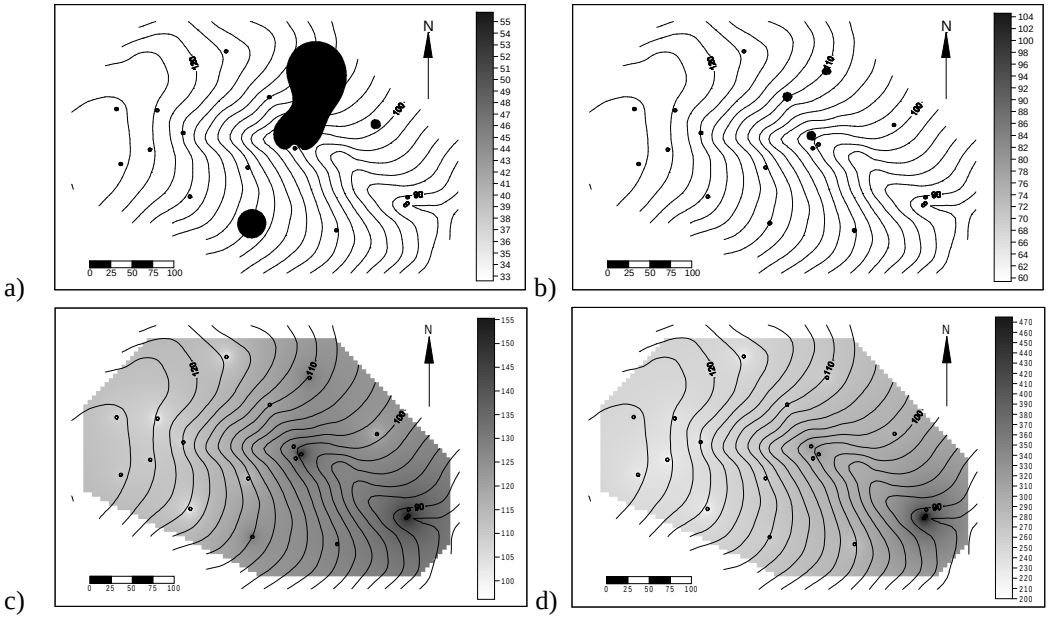

Figure 9.45: Plots of spatial variation in horizon depth (mm) across the Nerrigundah catchment for: a) horizon A1; b) horizon A2; c) horizon B1; and d) horizon B2. Circles indicate the location of horizon depth observations.

horizon thicknesses across the catchment is given by Figure 9.45. However, no obvious trend can be seen in these plots.

Figure 9.46 is a plot of the proportion of total soil depth comprised by the horizons A1, A2, B1 and B2, for soil profiles where all the horizons could be identified. The mean and standard deviation of these proportions are given on the figure. The values 10, 15, 25 and 50% of the total soil depth are used in Chapter 11 to describe the proportion of soil depth contained by horizons A1, A2, B1 and B2 for any location in the Nerrigundah catchment when estimating the spatial distribution in soil moisture content.

9.6.3 SOIL COLOUR

The soil colour gives an indication of whether the soil is undergoing oxidising or reducing conditions. A soil under reducing conditions is generally poorly aerated, poorly drained, wet and has grey coloration. A soil under oxidising conditions generally has orange coloration, indicating good aeration. The orange colour is due to the reaction of oxygen with metal ions (eg. iron forming iron oxide). The colour of the soil may also be used as an indication of the presence of organic matter. Soils rich in organic matter are characteristically

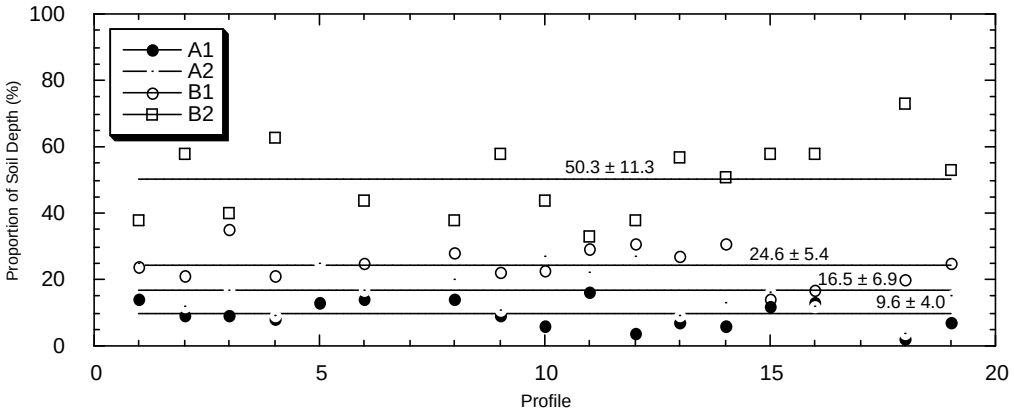

Figure 9.46: Proportion of total soil depth contained by horizons A1, A2, B1 and B2 for each soil profile. Mean and standard deviation are given on the figure.

dark in colour (ie. black or brown grey) (Hodgson, 1978) and have a greater water holding capacity (Macleod *et al.*, 1986).

The majority of soil profiles in the Nerrigundah catchment are dark (Figure 9.43). However, the depth of the dark layer varies considerably. Generally the darker coloration is found in the upper soil layers or A horizon. Soil profiles with dark coloration in the A horizon include 1, 6, 8, 9, 11, 14, 15, 16 and 19, which are located generally on hillslopes and in gullies. This dark coloration indicates a high proportion of organic matter, which is confirmed by the laboratory data (Table B.5). All of these profiles have 10% v/v or greater organic matter content in the A horizon. Profiles 10 and 13 (located on the hillslope and in the gully) respectively also have a dark A horizon, but less than 10% v/v organic matter content. The dark coloration in these profiles may in addition to organic matter be due to manganese (Hodgson, 1978). However, this has not been confirmed with laboratory tests.

Soil profiles 2, 3, 4, 5 and 7 are all pale in colour. From this it is assumed that they have low organic matter content. Except for soil profile 2, this is confirmed by the laboratory analysis, having less than 10% v/v organic matter. Low soil moisture content generally results in more pale soil colour. Hence the pale colour of profile 2 may be a result of its low soil moisture content. The pale coloration in these soil profiles may also be due to the presence of soil minerals such as silica, gypsum, calcium and magnesium (Hodgson, 1978), but this has not been confirmed with laboratory tests.

An important indicator of soil moisture conditions in regard to soil colour is mottling. A soil is said to be mottled using the Munsell standard soil colour charts (Oyama and Takehara, 1967) if it differs from the dominant colour by 5 units in hue, 2 units in value or 4 units in chroma (Morse *et al.*, 1982). Mottling is an indicator of seasonal water logging, resulting in combinations of greyish brown and reddish brown colours. Hence, a greater percentage of mottling indicates a greater duration of water logging. Observation of the soil profiles in Figure 9.43 revealed various degrees of mottling. Generally speaking, soil profiles on the ridge lines have a lesser amount of mottling than soil profiles in the gully. Soil profiles 9 and 18 have the greatest amount of mottling at 15%; soil profiles 2, 10 and 19 have 10% mottling; soil profiles 11 and 15 have 5% mottling; soil profiles 12, 13 and 14 have 3% mottling; soil profiles 1, 3 4, 8 and 17 have 2% mottling; and soil profiles 5, 6 and 16 have the least amount of mottling at approximately 1%.

The soil colour and mottling shown by several of the soil profiles allow for comments about the general soil moisture status of the soil in the Nerrigundah catchment.

- Soil profile 18 is fairly uniformly coloured throughout, being mostly grey and mottled with bright yellow brown. Hence this soil profile is likely to be under reducing or water logged conditions. This is consistent with its location near the catchment outlet.

- Soil profiles 10, 13 and 16 have very distinct boundaries between dark upper layers and lighter grey brown lower layers. The boundary is marked by a band of bright red brown. This therefore appears to be an oxidation/reduction boundary, indicating that the soil is rarely water logged above this boundary. This is also consistent with their locations, being on hillslopes.

- Soil profiles 12 and 17 do not contain any grey coloration. Hence there is no evidence of reducing or waterlogged conditions, suggesting that these profiles have very good drainage properties.

- Soil profile 6, located at the head of the gully, is distinctly different from most of the other soil profiles, in that the upper soil layers are lighter in colour than the lower soil layers. The dark coloration typical of high organic matter is lower in the soil profile and hence suggests that there is a high degree of leaching at this site.

- Soil profile 14, located midway along the gully, also shows darker coloration in the middle of the soil profile, rather than in the upper soil layer. However, this soil profile is much darker throughout the entire profile in comparison to soil profile 6. Hence, in addition to leaching, this is likely to be due to greater organic matter content along with reducing conditions, causing greyish colour rather than brighter orange and browns.

9.6.4 SOIL BULK DENSITY AND POROSITY

Soil bulk density is required for evaluation of the soil dielectric constant relationship in Chapter 2, while soil porosity is important for modelling soil moisture content, as this is the maximum amount of moisture storage for the soil. The laboratory results for soil bulk density and porosity are given in Table B.5.

Determination of soil bulk density involved drying the soil samples in an oven at 105°C, as bulk density is the oven dry weight of soil per unit volume (AS 1289.2.1.1, 1992). Thus, using the diameter of the corer and the depth of the horizon, the soil bulk density was determined. The soil's bulk density was then used to determine its porosity, as a soil's total porosity is the total amount of air and water which fills the pores within the soil (Hazelton and Murphy, 1992). The soil porosity ϕ was estimated from the soil bulk density ρ_b using the relationship

$$\phi = 1 - \frac{\rho_b}{\rho_s} \qquad (9.7),$$

where the specific gravity ρ_s was taken as 2.65 g cm^{-3}, being typical for most mineral soils (Freeze and Cherry, 1979). Typical values for bulk density and total porosity (see also Table B.8) of agricultural soil are 1.4 g cm^{-3} and 47% respectively (Hazelton and Murphy, 1992). The spatial variation of soil porosity across the catchment is given by Figure 9.47.

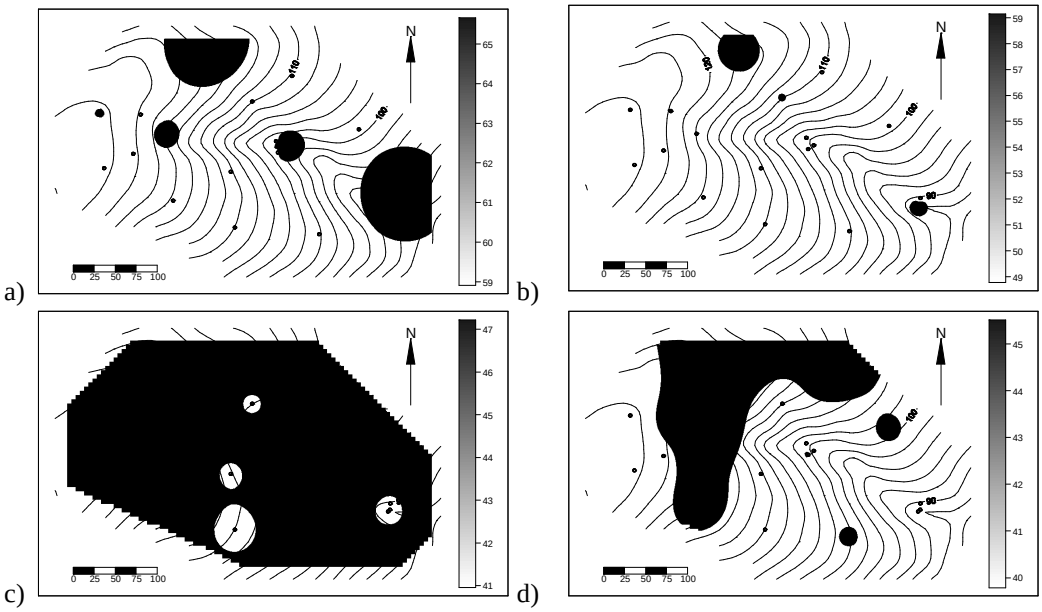

Figure 9.47: Plots of spatial variation in soil porosity (%) across the Nerrigundah catchment for: a) horizon A1; b) horizon A2; c) horizon B1; and d) horizon B2. Circles indicate sample locations.

9.6.5 SOIL ORGANIC MATTER CONTENT

The soil's organic matter content is necessary for estimation of the soil thermal conductivity and soil heat capacity, used for the estimation of soil heat flux. Organic matter content was determined by the method of ignition (Smith and Atkinson, 1975).

From the oven dried samples used for bulk density and soil porosity determination, a representative 10 g sample was taken. This was achieved by breaking up the sample with mortice and pestle, and halving with a sample divider box until the required sample size was obtained. This sample was then heated in an electric muffle furnace at 400°C for 24 hours, and gravimetric organic matter content determined by (Smith and Atkinson, 1975)

$$\%\ organic\ matter\ (\mathrm{g/g}) = \frac{initial\ weight\ sample - final\ weight\ sample}{initial\ weight\ sample} \times 100 \qquad (9.8).$$

Typical values for organic matter content are from 5 to 12% g/g for arable land, around 15% g/g for some horticultural soils under permanent pasture, and in excess of 50% g/g for peats and mor humus (Smith and Atkinson, 1975). Volumetric organic matter content was estimated from the gravimetric organic matter content by (de Vries, 1963)

Table 9.2: Soil composition for soil profile number 2.

Horizon	*Thickness (mm)*	*Porosity (% v/v)*	*Organic Matter (% v/v)*	*Quartz (% v/v)*	*Other Minerals (% v/v)*
A1	40	64.4	7.8	20.7	7.1
A2	55	41.1	4.7	33.0	21.2
B1	95	47.1	2.1	32.0	18.8
B2	260	32.3	3.3	33.0	31.4

$$\%\ organic\ matter\ (\mathrm{v/v}) = \%\ organic\ matter\ (\mathrm{g/g}) \times \frac{\rho_s}{\rho_{om}}(1-\phi) \qquad (9.9),$$

where the density of the organic matter (ρ_{om}) may be taken as 1.3 g cm^{-3} (de Vries, 1963). The organic content measurements for the Nerrigundah catchment are given in Table B.5.

9.6.6 SOIL QUARTZ CONTENT

The soils quartz content is needed for estimation of the soil thermal conductivity. Soil thermal conductivity is necessary for modelling soil temperature. Moreover, it was used for soil heat flux determination in section 9.5

From the 10 g soil sample used in the organic matter determination for soil profile 2, a further sub-sample was taken and ground up to a fine powder with mortice and pestle, for quartz content determination by X-Ray Diffraction. This test was only performed for the soil core taken near the weather station, where profile soil temperature and soil heat flux was monitored. The results from this analysis are given in Table 9.2.

9.6.7 PARTICLE SIZE ANALYSIS

Particle size analysis data is used for estimating the percentages of silt, sand and clay necessary for evaluation of the dielectric constant relationship given in Chapter 2. Moreover, particle size distribution may be used for soil texture assessment and hence estimation of soil properties such as saturated hydraulic conductivity.

The particle size analysis was performed on a sub-sample of between 100 and 200 g from the original oven dried samples, by halving with a sample divider box until the required sample size was obtained. The samples were then dispersed

Table 9.3: Particle size ranges (AS1289.3.6.1-1995).

Fraction	***Particle Size Limits***	***Equivalent AS Sieve Apertures***
Coarse Gravel	60 mm – 20 mm	63 mm – 19 mm
Medium Gravel	20 mm – 6mm	19 mm – 6.7 mm
Fine Gravel	6 mm – 2mm	6.7 mm – 2.36 mm
Coarse Sand	2 mm – 600 μm	2.36 mm – 600 μm
Medium Sand	600 μm – 200 μm	600 μm – 212 μm
Fine Sand	200 μm – 60 μm	212 μm – 75 μm
Coarse Silt	60 μm – 20 μm	
Medium Silt	20 μm – 6 μm	
Fine Silt	6 μm – 2 μm	
Clay	< 2μm	

overnight before wet sieving on the 75 μm sieve (AS 1289.3.6.2, 1995). A representative sub-sample of the particles passing the 75 μm sieve was obtained for particle size analysis of the silt and clay fractions by Laser Diffraction. The fraction remaining on the 75 μm sieve was collected and oven dried for dry sieving. The standard sieve sizes and corresponding soil fraction are given in Table 9.3.

Soil texture was determined from the percentages of clay, silt and sand (with sand taken as being sand plus gravel) using the soil texture triangle (Dingman, 1994). A summary of the results are given in Table B.6. A complete listing of particle size distribution for each sample tested is given in Appendix E,

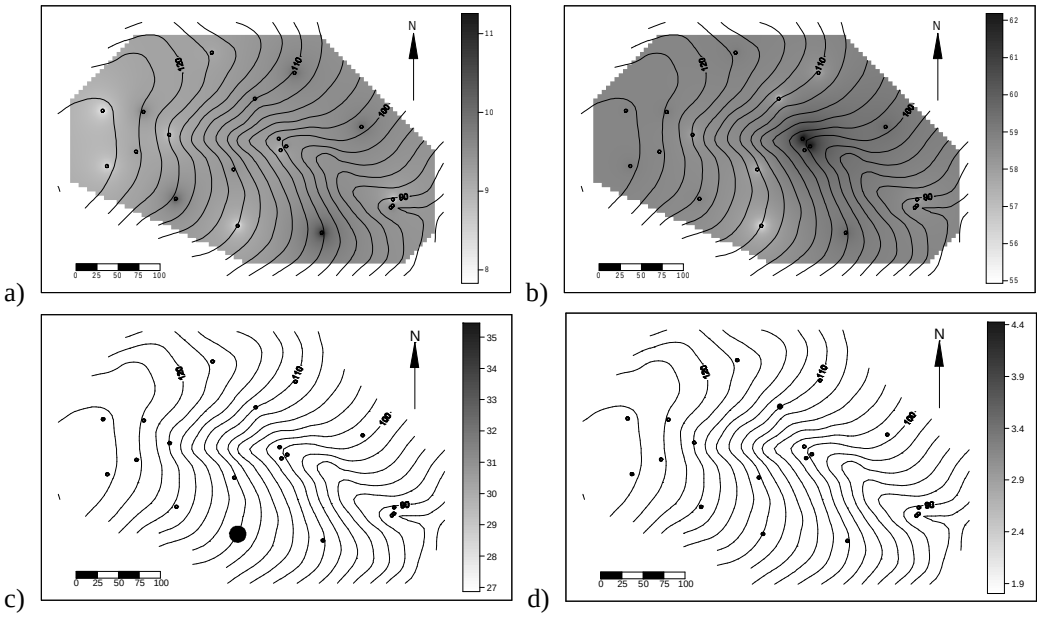

Figure 9.48: Spatial variation of: percentage a) clay; b) silt; c) sand; and d) gravel in the A1 horizon Throughout the Nerrigundah catchment. Circles show soil sample locations.

together with the grading curves. The spatial distributions of clay, silt, sand and gravel in the A1 horizon are given in Figure 9.48.

9.6.8 SATURATED HYDRAULIC CONDUCTIVITY

Saturated hydraulic conductivity is important for modelling soil moisture content, as it is a measure of how quickly water will travel through the soil under saturated conditions. In this section, saturated soil hydraulic conductivity has been estimated from the bulk density and particle size analysis of the soil cores taken throughout the Nerrigundah catchment with the TDAS, and compared with double ring infiltrometer and Guelph permeameter measurements at selected sites (Table B.7). The hydraulic conductivity estimates based on particle size have been made using the Kozeny-Carman equation (Bear, 1972; Freeze and Cherry, 1979), and literature values based on the soil texture triangle (Table B.13 and Table B.14).

The Kozeny-Carman equation is a semi-empirical relationship for estimating saturated hydraulic conductivity from particle size distribution and soil porosity. This equation was derived by treating the porous medium as a bundle of capillary tubes and solving the Navier-Stokes equation simultaneously for all capillary tubes passing through a cross-section normal to the flow. The unknown coefficient was then estimated from experimental data (Bear, 1972). The Kozeny-Carmen equation is given by (Freeze and Cherry, 1979)

$$K_s = \left(\frac{\rho g}{\mu} \right) \left[\frac{\phi^3}{(1-\phi)^2} \right] \left(\frac{d_m^2}{180} \right) \qquad (9.10),$$

where K_s is the saturated hydraulic conductivity (cm s^{-1}), ρ is the fluid density (g cm^{-3}), g is gravity (981 cm s^{-2}), μ is the fluid viscosity (g cm^{-1} s^{-1}), ϕ is the soil porosity, and d_m is a representative particle size (cm) taken as the median grain size. The spatial variation of saturated hydraulic conductivity as estimated by the Kozeny-Carmen relationship is given in Figure 9.49.

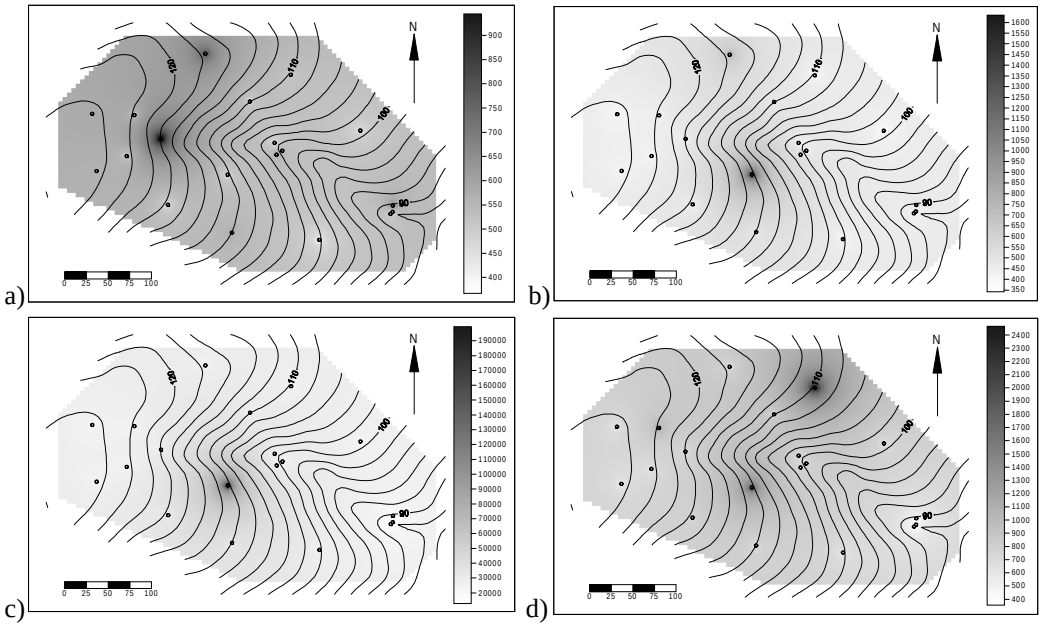

Figure 9.49: Spatial variation of Kozeny-Carmen estimate of saturated hydraulic conductivity (mm h^{-1}) throughout the Nerrigundah catchment for: a) A1 horizon; b) A2 horizon; c) B1 horizon; and d) B2 horizon.

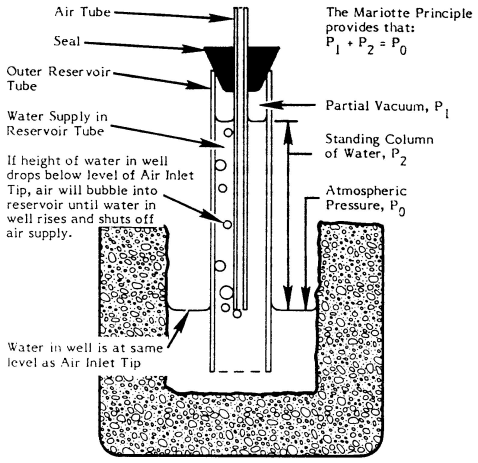

a) b)

Figure 9.50: a) Illustration of the Guelph permeameter operation; b) Illustration of the saturation bulb formed in the soil (Soil Moisture Equipment Corp, 1986).

The Guelph permeameter is an in-hole constant head permeameter, employing the Mariotte principle to maintain the constant head (Figure 9.50a). When a constant well height of water is established in a cored hole in the soil, a "bulb" of saturated soil with specific dimensions is quickly established (Figure 9.50b). This bulb is very stable and its shape depends on the type of soil, the radius of the well, and the head of water in the well. Once the unique bulb shape is established, the outflow of water from the well reaches a steady flow rate.

a) 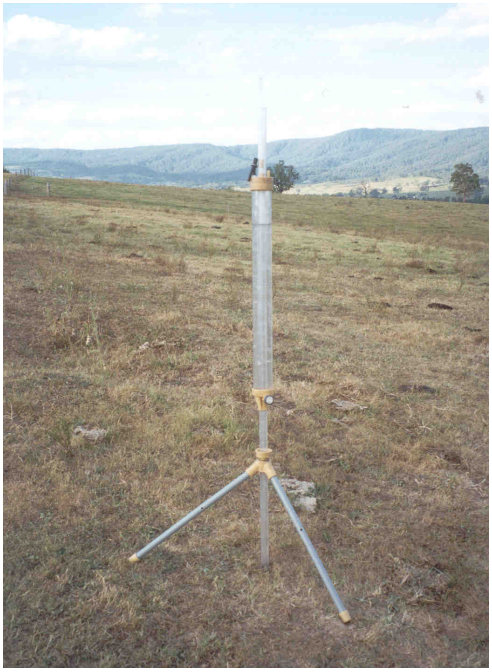 b) 

Figure 9.51: Photograph of a) Guelph permeameter and b) double ring infiltrometer.

By taking measurements at two different well heads, the saturated hydraulic conductivity can be estimated from the Richards equation, using the diameter of the well and rates of outflow at the two different well heads. It is suggested that well heads of 5 cm and 10 cm be established, with a minimum well depth of 15 cm (Soil Moisture Equipment Corp, 1986).

The double ring infiltrometer is designed to measure the saturated infiltration rate of the soil (Dingman, 1994). The outer ring (Figure 9.51b) provides a zone of saturated soil around the inner ring to buffer against lateral flow of soil moisture. Once the infiltration of water from the inner ring becomes constant, the saturated infiltration rate can be estimated. The major problem with the double ring infiltrometer for estimating soil hydraulic conductivity is that the infiltration rate is governed by the lowest hydraulic conductivity in the soil profile. Hence, one cannot be certain of the depth for which the infiltration measurement relates to the soil hydraulic conductivity.

9.6.9 PUBLISHED DATA

To model soil moisture requires the input of soil properties. Both laboratory and field procedures for determination of these properties are tedious,

time consuming and costly. Thus when soil properties are required for modelling of large areas comprising a variety of soil types, the feasibility of experimental efforts needs to be seriously considered. In view of the spatial variability of soil properties, the cost of adequate efforts may be prohibitive (Arya and Paris, 1981).

In addition to laboratory and field procedures, soil properties may be estimated from calibration of the hydrologic model. However, calibration procedures are time consuming and the data necessary for calibration are not always available. A feasible alternative is to use soils data that have already been collected for the area of interest. In New South Wales Australia, this data is kept in The Soils Data System, operated by the Department of Land and Water Conservation. Relevant soils data for the profiles nearest to the Nerrigundah catchment have been obtained and are given in Table B.9. The location of these profiles with respect to the Nerrigundah catchment is indicated in Figure B.14.

Actual saturated hydraulic conductivity values have not been provided for all soil profiles in Table B.9. Rather, saturated hydraulic conductivity has been given a rating, which may be interpreted by Table B.10.

Such detailed soils data as given in Table B.9 for soil profiles 63, 104, 140, 160, 179 and 182 (Figure B.14) is not always available. Rather, the soils data given for profiles 42, 64 and 75 may be more typical. This is because soil depth and texture may be readily determined in the field. In order for this data to be of use in modelling, relationships between soil hydrologic properties and soil texture are required. Table B.11 provides information on typical saturated hydraulic conductivity values while Table B.12 provides information on typical values for field capacity and wilting point (surrogate for residual soil moisture content). Table B.13 and Table B.14 provide information on typical values for soil porosity, saturated hydraulic conductivity and two commonly used water retention relationships (section 5.2.1). However, the large standard deviation within each textural class indicates that blind use of these average values may give erroneous values.

9.7 CHAPTER SUMMARY

This chapter has presented the data collected in the Nerrigundah experimental catchment, for evaluation of the soil moisture profile estimation algorithm in Chapters 10 and 11. This data includes near-surface soil moisture observations for updating of the hydrologic model, soil moisture profile data for calibration of the hydrologic model, and soil moisture profile data for evaluation of the soil moisture profile estimation algorithm. Moreover, the surface moisture flux data necessary for forcing of the soil moisture model, and the elevation data and soil data necessary for input to the forecasting model has been presented. In addition, published elevation data and soil data quality and availability has been investigated, as this is the data that would be used in a near-real-time application of the soil moisture profile estimation algorithm.